Title

Acute adenoviral infection elicits an arrhythmogenic substrate prior to myocarditis.

Authors and Affiliations

Rachel L. Padget[1,2,3], Michael J. Zeitz[2,3], Grace A. Blair[1,2,3], Xiaobo Wu[2,3], Michael D. North[4], , Mira T. Tanenbaum[4], Kari E. Stanley[1,2,3], Chelsea M. Phillips[2,3], D. Ryan King[1,2,3], Samy Lamouille[2,3,4,5,7], , Robert G. Gourdie[2,3,4,6], Gregory S. Hoeker[2,3], Sharon A. Swanger[2,4,5], Steven Poelzing[2,3,4,6], James W. Smyth[2,3,4,6,7]

[1] Graduate Program in Translational Biology, Medicine, and Health, Virginia Tech, Blacksburg, VA 24061, USA
[2] Fralin Biomedical Research Institute at Virginia Tech Carilion, Roanoke, VA 24016, USA
[3] Center for Vascular and Heart Research, FBRI at VTC, Roanoke, VA 24016, USA
[4] Virginia Tech Carilion School of Medicine, Roanoke, VA 24016, USA
[5] Department of Biomedical Sciences and Pathobiology, Virginia-Maryland College of Veterinary Medicine, Virginia Tech, Blacksburg, VA 24061, USA
[6] Department of Biomedical Engineering and Mechanics, College of Engineering, Virginia Tech, Blacksburg, VA 24061, USA
[7] Department of Biological Sciences, Virginia Tech, Blacksburg, VA 24061, USA

Short Title

Arrhythmogenic adenoviral cardiac infection

Corresponding author

James W. Smyth,
Fralin Biomedical Research Institute at VTC,
2 Riverside Circle,
Roanoke,
VA 24016.
Email: smythj@vtc.vt.edu

Total word count: 14,050

Abstract

Background: Viral cardiac infection represents a significant clinical challenge encompassing several etiological agents, disease stages, complex presentation, and a resulting lack of mechanistic understanding. Myocarditis is a major cause of sudden cardiac death in young adults, where current knowledge in the field is dominated by later disease phases, and pathological immune responses. However, little is known regarding how infection can acutely induce an arrhythmogenic substrate prior to significant immune responses. Adenovirus is a leading cause of myocarditis, but due to species-specificity, models of infection are lacking and it is not understood how adenoviral infection may underlie sudden cardiac arrest. Mouse Adenovirus Type-3 (MAdV-3) was previously reported as cardiotropic, yet has not been utilized to understand mechanisms of cardiac infection and pathology.

Methods: We have developed MAdV-3 infection as a model to investigate acute cardiac infection and molecular alterations to the infected heart prior to an appreciable immune response or gross cardiomyopathy.

Results: Optical mapping of infected hearts exposes decreases in conduction velocity concomitant with increased Cx43Ser368 phosphorylation, a residue known to regulate gap junction function. Hearts from animals harboring a phospho-null mutation at Cx43Ser368 are protected against MAdV-3 induced conduction velocity slowing. Additional to gap junction alterations, patch clamping of MAdV-3-infected adult mouse ventricular cardiomyocytes reveals prolonged action potential duration as a result of decreased I_{K1} and I_{Ks} current density. Turning to human systems, we find human adenovirus type-5 (HAdV-5) increases phosphorylation of Cx43Ser368 and disrupts synchrony in human induced pluripotent stem cell-derived cardiomyocytes (iPSC-CMs), indicating common mechanisms with our mouse whole heart and adult cardiomyocyte data.

Conclusions: Together, these findings demonstrate that adenoviral infection creates an arrhythmogenic substrate through direct targeting of gap junction and ion channel function in the heart. Such alterations are known to precipitate arrhythmias and likely contribute to sudden cardiac death in acutely infected patients.

Non-standard Abbreviations and Acronyms

ACM	Adult mouse ventricular cardiomyocyte
APD	Action potential duration
cTNI	Cardiac Troponin I
Cx43	Connexin43
CV	Conduction velocity
CVB3	Coxsackievirus B3
CVL	Longitudinal conduction velocity
CVT	Transverse conduction velocity
DCM	Dilated cardiomyopathy
ECG	Electrocardiogram
EF	Ejection fraction
FS	Fractional shortening
GJIC	Gap junction intercellular communication
HPV	Human papillomavirus
HSV	Herpes simplex virus
HAdV-5	Human adenovirus type-5
HF	Heart failure
HiPSC-CM	Human induced pluripotent stem cell derived cardiomyocyte
HRP	Horseradish peroxidase
ID	Intercalated disc
IFN	Interferon
LQT	Long QT syndrome
LV	Left ventricle
LVDP	Left ventricular developed pressure
MAdV-3	Mouse adenovirus type-3
MOI	Multiplicity of infection
NMuMG	Normal murine mammary gland epithelial cells
NMVCM	Neonatal mouse ventricular cardiomyocyte
SCD	Sudden cardiac death
ZO-1	Zonula occludens-1

Introduction

Viral infection of the heart results in significant morbidity and mortality, representing a major cause of sudden cardiac death (SCD) in young adults where up to a 42% causative incidence of viral-associated myocarditis is reported[1-3]. Viral myocarditis is classified into distinct phases of disease, encompassing an acute phase of active infection where direct viral-mediated damage to myocardial cells occurs and may subsequently progress to a chronic disease phase involving the host immune response[4]. Chronic viral myocarditis can then advance to dilated cardiomyopathy (DCM) and heart failure, with limited clinical options available bar the supportive care and potential need for transplant shared with other forms of end-stage cardiac disease[5,6]. Clinical myocarditis data are understandably dominated by chronic disease, where host immune responses to the initial infection are understood to precipitate pathological remodeling to HF[7]. The molecular mechanisms of acute cardiac infection, and specifically how active viral replication in the myocardium precipitates arrhythmia prior to an appreciable immune response, are not well understood. Indeed, individuals with such direct active cardiac involvement often do not survive the sudden cardiac arrest event triggered by infection and/or do not present with altered cardiac remodeling and function by echocardiography, for example[8,9]. A better understanding of how acute viral infection alters cardiac electrophysiology and function prior to immune infiltration is key in the development of interventions against arrhythmogenesis, in addition to identifying pathways underlying progression to chronic viral myocarditis for therapeutic targeting and/or early diagnosis.

Arrhythmias, while rare, are the leading cause of sudden cardiac arrest in children and young adults[3,10,11]. Hypertrophic obstructive cardiomyopathy and congenital abnormalities are significant contributors to SCD in such cases, but here we investigate how acute viral infection can elicit pathological remodeling preceding SCD in hearts otherwise devoid of such apparent cardiomyopathy. Normal cardiac electrophysiological function is achieved primarily through two major components: ion channels localized to specific nanodomains of the sarcolemma, and cell-to-cell electrical coupling at the intercalated disc (ID)[12-14]. The proteins comprising the major cardiac ion channels responsible for generation of the action potential (AP), including $Ca_V1.2$, $Na_V1.5$, Kir2.1, $K_V7.1$, and $K_V11.1$, are subject to dynamic regulation affecting their localization and function. Pathological alterations to the AP, such as prolonged duration due to perturbed channel function, can lead to lethal arrythmias[15]. IDs encompass fascia adherens, gap junctions, the perinexus, desmosomes, and an enrichment of several ion channels to effect mechanical and electrical coupling between adjacent cardiomyocytes[16-21]. Subcellular remodeling of such ID-resident structures and channels is well described as underlying arrhythmogenesis across a breadth of cardiac disease states, including viral infection[22-27].

A rapid and modifiable mechanism of regulating structures at the ID is dynamic phosphorylation of target proteins. A common outcome of increased phosphorylation of gap junctions and ion channels is a positive or negative effect on function[28-30]. In addition to direct impacts, indirect consequences include regulation of ion channel density. For example, increased phosphorylation by PKC on KCNE1 can impair trafficking of the KCNQ1/KCNE1 complex forming the ion channel, $K_V7.1$, and therefore reduce I_{Ks}[31,32]. Changes to gap junction intracellular communication (GJIC) are established in underlying arrhythmias and SCD[33]. Twenty-one human connexins have been identified, with connexin43 (Cx43) being the most ubiquitously expressed throughout the body while also being the primary connexin of the ventricular working myocardium[34]. In addition to electrical coupling, gap junctions play a critical role in propagation of innate and adaptive antiviral immune responses, providing justification for pathogens to target such structures[35-37]. Indeed, we have previously reported Cx43 is specifically down regulated at the transcriptional level and functionally targeted through altered

158 phosphorylation during adenoviral infection in human epithelial cells and induced pluripotent
159 stem cell-derived cardiomyocytes (HiPSC-CMs)[38].
160
161 The most common viral families identified as causative agents in SCD and development of viral
162 myocarditis include adenoviruses, enteroviruses (Coxsackievirus B3, CVB3), herpesviruses,
163 and parvoviruses, with enteroviruses representing the most intensely researched[10,39,40]. SARS-
164 CoV-2 infection has also been implicated both directly and indirectly in myocarditis
165 development[40,41]. Regarding enteroviruses, CVB3 is a non-linear, positive-sense single-
166 stranded RNA (ssRNA) virus from the picornavirus family commonly associated with childhood
167 illness and a significant causative agent of viral myocarditis in all ages[42]. The ability of CVB3 to
168 viably infect and replicate across species has resulted in its development as a valuable, and
169 arguably leading, research model for viral myocarditis[27,43,44]. Indeed, the majority of viral
170 myocarditis research has been conducted using CVB3 with an emphasis on the chronic phase
171 of disease[7]. Other viruses known to cause myocarditis, such as adenoviruses, have starkly
172 different biology to CVB3, perhaps most obviously is their double stranded DNA (dsDNA)
173 genomes requiring the virus to colonize the cellular nucleus and uncouple cell cycle regulation
174 for a significantly longer life cycle than a positive-sense RNA virus[42,45,46]. Such differences likely
175 elicit virus-specific pathologies during the acute stage of viral myocarditis, illustrating the need to
176 investigate virus family-specific disease progress and pathology beyond CVB3.
177
178 Adenoviruses are non-enveloped, dsDNA viruses, and include over 50 serotypes (now 'types')
179 capable of human infection where they cause a range of illnesses from mild respiratory disease
180 to more severe and potentially fatal conditions such as myocarditis[47]. Tissue tropism is
181 classically attributed to type-specific host cell receptor binding and/or permissiveness of specific
182 cell types to adenoviral replication[48]. Human adenovirus types 2 and 5 (HAdV-2 and -5) are the
183 most predominant causes of adenoviral myocarditis, although additional types are increasingly
184 reported[49-51]. Early adenoviral proteins mimic growth factor signaling and induce cell cycle entry
185 to take advantage of DNA synthesis machinery and replicate viral genomes[46,52,53]. These same
186 signaling pathways target GJIC, as we have previously demonstrated, and likely also impact the
187 cardiac ion channels that shape the AP[28,31,38,54]. Unlike CVB3 however, many HAdVs cannot
188 replicate effectively in mice, resulting in a dearth of understanding regarding adenoviral
189 cardiotropism and virus-specific effects on the heart due to this stringent adenoviral species-
190 specificity[47,55]. Mouse adenovirus type 1 (MAdV-1) has historically been employed in modeling
191 respiratory disease and encephalitis, and while not a 'cardiotropic' virus, additional studies have
192 successfully modeled adenoviral myocarditis in mice using MAdV-1, with an emphasis on
193 inflammation[56-59]. In 2008, mouse adenovirus type-3 (MAdV-3) was isolated as distinct from the
194 previously described MAdV-1 and MAdV-2, and reported to be cardiotropic[60,61]. Development of
195 MAdV-3 as a model for myocarditis, or use of this virus in investigation mechanisms of
196 arrhythmogenesis during acute cardiac infection has been limited, however.
197
198 In this study, we successfully employ MAdV-3 to model acute viral cardiac infection in adult
199 mice and confirm similar targeting of Cx43 to that which we previously observed with human
200 adenovirus[38]. While we do report induction of a cardiac antiviral immune response at the RNA
201 level and increases in infiltrating macrophages, , we find slowed conduction velocity in infected
202 hearts and prolonged AP duration (APD) in infected cardiomyocytes; two pro-arrhythmogenic
203 phenotypes occurring prior to appreciable adaptive immune cell infiltration or development of
204 any gross cardiomyopathy. Importantly, our cell-based studies reveal electrophysiological and
205 gap junction disturbances independent of a host immune system. Turning to studies in isolated
206 primary adult cardiomyocytes we identify perturbation of I_{KS} and I_{K1} underlies prolonged APD
207 during adenoviral infection. MAdV-3 infection therefore represents a viable and relevant model
208 of acute myocarditis, and targets cardiac conduction through the same mechanisms we have

209 previously found in cell-based human adenovirus studies. While we focus on an acute stage of
210 7 days post infection where presumably some inflammatory processes and cytokine effects will
211 have initiated, significant adaptive immune cell infiltration and/or cardiomyocyte damage is not
212 occurring at a detectable level. Our data demonstrate that acutely infected hearts harbor
213 dangerous electrophysiological alterations at the molecular level and reveal, for the first time,
214 how adenoviral infection can precipitate such pathological subcellular remodeling prior to
215 cardiomyopathy and development of inflammatory myocarditis.

Materials and Methods

All materials and methods are described in the Supplemental Material and Major Resources Table.

Results

Mouse adenovirus type-3 is cardiotropic and does not invoke an appreciable infiltrative cardiac immune response during acute infection.

We previously reported specific targeting of Cx43 expression and gap junction function during adenoviral infection[38]. Such alterations in Cx43 would significantly impact cardiac electrophysiology directly through affecting GJIC, while potentially indirectly impacting sodium channels and/or other key components of arrhythmogenesis[19,21,62,63]. Despite significant incidence of adenoviral myocarditis, establishment of an adult mouse disease model has been elusive due to species-specificity[55]. We first sought to examine the potential of MAdV-3 as a model of acute cardiac infection, given the prior reports of cardiotropism[60]. To test this, 8-12 week old male and female C57BL/6 mice were inoculated with 5 x 10^5 i.u. MAdV-3 via retro-orbital injection. Animals were sacrificed and organs harvested 7 d.p.i. for histology and DNA isolation. Using qPCR we find MAdV-3 viral genomes significantly enriched only within cardiac tissue and spleen (log fold-change heart relative to lung 2.1, spleen 0.78), confirming cardiotropism (Figure 1A). A similar time-course over 7 days focusing on cardiac tissue alone reveals levels of viral genomes plateauing from 3-7 d.p.i., consistent with active viral replication in the heart during this time (Figure 1B). No weight loss or apparent evidence of malaise (e.g. hunching, fur-ruffling) were observed in infected animals during the 7 day time course (data not shown). We then employed RNA sequencing of control and MadV3 infected ventricular tissue from mice to assess global transcriptional changes (Figure 1C). MadV3 infected ventricles had 321 significant differentially expressed genes in comparison to controls. Nearly all (99%) differentially expressed genes were upregulated in response to viral infection. Differentially expressed genes were hierarchically clustered using the clustergrammer[64] web program and are presented as a heatmap. To determine enriched gene ontology terms, over-representation analysis was performed with the significant differentially expressed genes using ClusterProfiler[65]. The top 10 most significant gene ontology terms for biological processes are shown sorted by gene ratio. Gene ontology of biological processes indicated an enrichment of immune related genes comprising both innate and adaptive immune responses in MAdV-3 infected ventricular tissue. Histopathology, however, revealed no gross pathology or appreciable infiltration of leukocytes in infected cardiac tissue (Figure S1A). To measure infiltration more specifically, we performed confocal microscopy immunofluorescence labeling of ventricular myocardial cryosections for the major immune cell markers: F4/80 (macrophages), CD3 (T-cells), and CD45R/B220 (B-cells, NK cells, CTLs). While increased numbers of F4/80+ cells were detected in MAdV-3 infected hearts, no changes to CD3+ or CD45R+ cell numbers were found in ventricular tissues, with CD3+ cells being notably rare (Figure 1D,E; Figure S1B,C). A lack of direct cardiomyocyte damage and presence of a cardiac inflammatory response were confirmed by serum cardiac troponin I (cTnI) ELISA and cytokine array on heart protein lysates, respectively, where no significant changes were detected between groups (Figure S1D; Figure S2). Gross spleen weight, however, was higher in infected mice (83.3 ± 5.58 mg vs.133.5 ± 7.45 mg, mean ± SEM; Figure S1E). To measure humoral anti-MAdV-3 responses, we employed an ELISA to quantify anti-MAdV-3 IgG and find that while a significant response has been initiated at 7 d.p.i., this does not plateau until after 21 d.p.i. (Figure S1F). Together, these findings confirm that MAdV-3 is cardiotropic, representing a relevant model of acute viral myocarditis to examine mechanisms of arrhythmogenesis. While anti-viral immune responses have been initiated at 7 d.p.i, inflammatory cytokines are not detectable in the heart at the protein level. With no significant myocardial tissue damage or adaptive cellular infiltration, we conclude this

stage of cardiac infection to be prior to appreciable direct host immune-mediated damage or cardiomyopathy, and faithful to reported presentation of such cardiac infections in humans[8].

Cardiac conduction velocity is slowed during acute adenoviral infection in the absence of apparent cardiomyopathy.

Data in Figure 1 confirm MAdV-3 cardiotropism in mice, and identify 7 d.p.i. as a timepoint where viral replication has been occurring in the heart for several days while detectable adaptive immune infiltration and/or cardiomyopathy have not yet occurred. Consistent with this, by echocardiography we find no detectable changes in ejection fraction, left ventricle developed pressure at diastole, or fractional shortening by echocardiography in infected animals compared to controls (Figure 2A). Given cases of SCD with acute viral involvement often involve essentially normal heart structure at the gross level, we next asked how cardiac electrophysiology may be affected during MAdV-3 infection. Infected and control animals were anesthetized and, using electrode pads, baseline electrocardiograms (ECGs) revealed no alterations to the PR, QRS, or QT intervals in MAdV-3-infected mice compared to mock-infected animals (Figure 2B-E). A significant prolongation of the R-R interval (114.4 ± 0.98 ms, MAdV-3 infected mean 121.4 ± 1.77 ms, mean ± SEM), indicative of bradycardia, was detected in infected animals, however (Figure 2F). To assess alterations in intercellular coupling, we next turned to measurement of conduction velocity (CV) by optical mapping. Excised hearts from infected and control animals were Langendorff-perfused and optical mapping performed to quantify longitudinal and transverse CV (CVL and CVT, respectively) during steady-state perfusion (Figure 3). While CVL was similar in both groups, we find significant CVT slowing in MAdV-3-infected hearts in comparison to mock-infected controls (38.75 ± 2.60 vs. 29.33 ± 2.88 cm/s, mean ± SEM, respectively: Figure 3C). Such reductions in ventricular conduction velocity are known to underlie arrhythmogenesis and mechanistically are typically associated with perturbation of gap junction function and/or connexin expression[17,62,66-70].

Aberrant connexin43 phosphorylation is induced in MAdV-3 infected hearts and primary cardiomyocytes.

Having identified a conduction defect in MAdV-3 infected hearts, we next examined expression of proteins critical to cardiac electrophysiology, cardiomyocyte ID structure, and gap junction formation and maintenance. Turning to our RNA-Seq data (Figure 1C) we find no changes to expression levels of major cardiac connexins, major cardiac ion channels/subunits, or structural genes *Tjp1*, *Cdh2*, and *Pkp2* (Figure S3). We therefore investigated post-transcriptional alterations that could underlie the conduction slowing presented in Figure 3. Previously, we found a decrease of Cx43 protein localization at the cell-cell border during HAdV-5 infection in HaCaT and HiPSC-CMs[38]. To ask if gap junction localization at the ID was affected in MAdV-3 infected mouse hearts, we performed confocal immunofluorescence microscopy on myocardial cryosections to visualize Cx43 distribution in ventricular cardiomyocytes. Through quantification of Cx43 intensity at the ID, as determined through colocalization with N-cadherin[26,71,72], we find no significant losses in gap junction localization between infected or control hearts (Figure 4A). Levels of Cx43 protein were also comparable by western blotting of lysates from MAdV-3 infected versus control cardiac tissue lysates at 7 d.p.i. (Figure 4B). Given our finding of slowed CVT without detectable alterations in Cx43 protein expression or localization, we assessed the post-translational status Cx43. Specifically, phosphorylation of $Cx43^{Ser368}$ results in reduced channel opening probability, and our prior work with HAdV-5 identified this residue as being hyperphosphorylated during adenoviral infection of human epithelial cells[29,30,38]. Consistent with this, we find induction of $Cx43^{Ser368}$ phosphorylation by western blotting of ventricular lysate from mice infected 7 d.p.i. with MAdV-3 in comparison to mock-infected animals (1.16 ± 0.11 vs. 1.57 ± 0.15, mean ± SEM) (Figure 4B). To ask if MAdV-3 induces $Cx43^{Ser368}$ phosphorylation *in vitro*, we isolated primary mouse neonatal cardiomyocytes and infected them at an MOI of 10 with

MadV-3 for 24 h. Induction of Cx43^{Ser368} phosphorylation was detected *in situ* by confocal immunofluorescence microscopy (Figure 4C). While control cells displayed some Cx43^{368} phosphorylation (green), most connexin detected was not phosphorylated at this residue (magenta). The majority of Cx43 detected in MAdV-3 infected cells however was positive for Ser368 phosphorylation. Quantification relative to total Cx43 reveals significant induction of Cx43^{Ser368} phosphorylation in primary neonatal cardiomyocytes compared to controls (0.98 ± 0.05 vs. 1.40 ± 0.04, mean ± SEM), importantly demonstrating infection alone is sufficient to induce this in the absence of host antiviral immune response.

Adenoviral infection prolongs adult cardiomyocyte action potential duration through perturbation of potassium currents.

Proper cardiac electrophysiology depends not just upon intercellular coupling and AP propagation, but the repetitive formation and resolution of consistent AP morphology through the dynamic actions of several ion channels[12]. Although no alterations in cardiac ion channel gene expression were detected by RNA-Seq and RTqPCR (Figure S3), given that we also found no change to Cx43 mRNA or protein levels, but significantly altered GJ function in infected hearts (Figure S3, Figure 4); we sought to investigate changes to electrophysiology during MAdV-3 infection. Next, we employed patch-clamping as a non-biased approach in measuring changes to cardiomyocyte electrophysiology during infection. Primary adult mouse ventricular cardiomyocytes were infected immediately post-isolation with MAdV-3 at a multiplicity of infection (MOI) of 10 or mock-infected and incubated for 24 h prior to experimentation. Importantly, infected cells were viable at this timepoint with no apparent cytopathic effect noted. Using confocal immunofluorescence microscopy, 100% infection was confirmed using MAdV-3 antiserum, where infected cells are noted to have maintained normal structure (data not shown). First, we performed whole-cell current clamp to determine if AP morphology was altered during MAdV-3 infection. While no alterations in depolarization rate (rise time/max rise slope) were detected, significant APD prolongation occurs in MAdV-3 infected cells relative to uninfected controls presented here through increased APD90 (13.87 ± 0.63 ms vs. 17.02 ± 0.67 ms, mean ± SEM) and decay time (6.03 ± 0.31 ms, 8.60 ± 0.57 ms, mean ± SEM) concomitant with decreases in max decay slope (-34.31 ± 2.82 ms vs. -26.17 ± 1.90 ms, mean ± SEM) and afterpolarization (AHP) amplitude (-1.92 ± 0.20 mV vs. -1.30 ± 0.19 mV, mean ± SEM) (Figure 5A-D). Having identified such pathological APD prolongation, we next utilized whole-cell voltage-clamp to assess individual currents and isolate the specific cardiomyocyte ion channels affected during MAdV-3 infection. No alterations in I_{Na} or I_{Ca} were detected in MAdV-3 infected ACMs (Figure 6A,B). The AP morphology changes we report occur during phases 3 and 4, however, leading us to focus in more detail on the potassium currents which primarily control proper repolarization and AP resolution. While no difference in I_{Kr}, or I_{Ks} peak currents were detected between control and infected ACMs, I_{Ks} tail current differences (50 mV; -4.50 ± 0.64 pA/pF vs -3.15 ± 0.53 pA/pF, 55 mV; -5.03 ± 0.58 pA/pF vs. -3.16 ± 0.53 pA/pF, 60 mV; -4.03 ± 0.56 pA/pF MAdV-3 mean average -3.27 ± 0.52 pA/pF, mean difference ± SEM) and I_{K1} peak current (-19.80 ±1.99 pA/pF vs. -12.24 ± 1.61 pA/pF, mean ± SEM) were significantly perturbed during MAdV-3 infection (Figure 6C-E, Figure S4B,C). These data reveal potentially arrhythmogenic APD prolongation occurs in infected ventricular cardiomyocytes, compounding the electrophysiological disturbances we report affecting conduction velocity and cardiac gap junction function during acute MAdV-3 infection of the heart.

Human Adenovirus Type-5 increases Cx43^{Ser368} phosphorylation through PKC activation and uncouples HiPSC-derived cardiomyocytes.

We previously reported that HAdV-5 disrupts expression and function of Cx43 in human epithelial cells and complexing of Cx43 with ZO-1 in HiPSC-CMs[38]. To translate our current findings of GJIC disruption and CV slowing in MAdV-3 infected mouse hearts (Figure 3, Figure

369 4) to a human model system, we investigated how functional intercellular coupling and Cx43
370 phosphorylation might be altered in HAdV-5 infected HiPSC-CMs. Matured HiPSC-CMs were
371 cultured and infected with human adenovirus type-5 (HAdV-5) or with HAd-LacZ, a replication
372 incompetent human adenovirus serving as control, at an MOI of 10. Phosphorylation of
373 $Cx43^{Ser368}$ is well established to occur via PKC[29,30,73-77]. To test if PKC activity is required for
374 $Cx43^{Ser368}$ phosphorylation during adenoviral infection we utilized two separate PKC inhibitors
375 (sotrastaurin/AEB071[78,79] 'S'; or bisindolylmaleimide VIII/Ro 31-7549[80] 'B') 1 h post infection (to
376 ensure kinase inhibition would not hinder viral update). Just as we see with MAdV-3 in hearts
377 and primary mouse cardiomyocytes (Figure 4B,C), HAdV-5 infection induces $Cx43^{Ser368}$
378 phosphorylation at 24 h.p.i. when compared to HAd-LacZ controls (2.23 ± 0.26 vs. 12.38 ± 3.03,
379 mean ± SEM), though not significant following the use of non-parametric testing due to small
380 sample size. (Figure 7A). Importantly, both B and S inhibitors completely ablated this response,
381 confirming PKC activity is necessary for $Cx43^{Ser368}$ phosphorylation during adenoviral infection.
382 To assess the impact of infection on electrical coupling, monolayers were loaded with the
383 calcium sensitive Fluo4-AM 24 h.p.i. and live-cell confocal microscopy performed at 166 Hz to
384 visualize spontaneous calcium transients. After imaging, cells were fixed and 100% infection
385 confirmed through immunofluorescence labeling of the early HAdV-5 protein E1A (Figure 7B).
386 While HAd-LacZ (control) HiPSC-CMs consistently displayed synchronous firing across the
387 monolayer, uncoupling of HAdV-5 infected cells is demonstrated through significant cell-to-cell
388 variability in time to max peak intensity (56.69 ± 8.68 ms vs. 123.8 ± 20.21 ms, mean ± SEM)
389 (Figure 7C,D; Video S1 and Video S2). Therefore, just as we find in our MAdV-3 *in vivo* and *in*
390 *vitro* studies, HAdV-5 infection disrupts cardiomyocyte electrical coupling independent of a host
391 immune response, confirming that acute adenoviral infection generates dangerous electrical
392 disturbances in still-viable cardiomyocytes which likely contribute to the arrhythmias of SCD
393 attributed to acute viral myocarditis.
394
395 **The phospho-null $Cx43^{S368A}$ mutation protects against cardiac conduction slowing during**
396 **acute MAdV-3 infection.**
397 We identified increases in $Cx43^{Ser368}$ phosphorylation in MAdV-3 infected hearts where
398 conduction slowing was occurring (Figure 3) and in HAdV-5 infected HiPSC-CMs displaying
399 dyssynchronous firing (Figure 7). To test if prevention of $Cx43^{Ser368}$ phosphorylation could
400 protect infected hearts from such perturbations, we utilized transgenic mice harboring a
401 Serine368 to Alanine mutation Cx43[81]. Complete loss of $Cx43^{Ser368}$ phosphorylation in hearts
402 from MAdV-3 infected $Cx43^{S368A}$ animals was confirmed by western blot and compared to wild-
403 type animals as a positive control (Figure 8A). As with wild-type animals, excised hearts from
404 infected and control animals were Langendorff-perfused and optical mapping performed to
405 quantify CVL and CVT during steady-state perfusion. We find no significant changes in CVL or
406 CVT between control and MAdV-3-infected hearts from $Cx43^{S368A}$ mice, indicating this mutation
407 is protective against virally-induced conduction slowing during acute cardiac infection (Figure
408 8B-D).
409
410 **Discussion**
411
412 By definition, viral myocarditis encompasses inflammation and a significant contribution to either
413 gross or molecular myocardial alterations due to infiltration of host immune cells and associated
414 cytokine signaling[82]. There is, however, a significant gap in our understanding of pathologic
415 events that occur during acute cardiac infection, prior to development of any detectable
416 cardiomyopathy or mounting the infiltrative host antiviral immune response[83]. In this study, we
417 implement MAdV-3 as a model cardiotropic adenovirus to isolate virally induced mechanisms of
418 arrhythmogenesis during initial/acute infection that precede myocarditis or chronic disease
419 development. While historically understudied in the context of cardiovascular disease,

420 adenoviruses are a leading causative agent of myocarditis with the majority of cases seemingly
421 reported in young adults and children[84]. Moreover, adenoviral genomes have been detected in
422 cardiac tissue in cases of SCD where gross structural changes of the myocardium are not
423 apparant[85]. While we cannot rule out immune-mediated effects completely, we report that, prior
424 to an appreciable infiltrative adaptive immune response and/or damage to cardiac tissue;
425 adenoviral infection decreases potassium current density leading to prolonged action potential
426 duration with concurrent reductions in gap junction intercellular communication affecting
427 conduction.
428
429 Connexins participate in propagation of, but are also subject to regulation by, inflammatory
430 responses[35,36,86]. Thus, it is important in this study to parse out viral- versus host immune
431 response-mediated induction of the arrhythmogenic substrate during acute viral infection. *In*
432 *vitro*, we observe increased $Cx43^{Ser368}$ phosphorylation in MAdV-3 infected isolated primary
433 cardiomyocytes and HadV-5 infected HiPSC-CMs, two experimental preparations confirming
434 phosphorylation of $Cx43^{Ser368}$ can occur during infection independent of host immune responses
435 (Figure 4C; Figure 7). Similarly, our patch clamping data in primary adult cardiomyocytes also
436 demonstrate prolonged APD with disruption of potassium currents occur in infected
437 cardiomyocytes in the absence of a host immune system (Figure 5; Figure 6). *In vivo*, we do not
438 detect evidence of inflammation or cardiac damage, adaptive leucocyte infiltration, or increased
439 cytokine levels at the protein level in MAdV-3 infected hearts (Figure 1D,E; Figure S1A-D;
440 Figure S2). A primary finding of our study is hyperphosphorylation of $Cx43^{Ser368}$ during infection
441 to affect GJIC. Regarding specific cytokine effects, previous research has shown that increased
442 IL-1β can prolong the QRS complex and induce $Cx43^{Ser368}$ phosphorylation in an *ex vivo*
443 myocarditis model in rats[87]. We find no significant difference in downstream targets of IL-1β via
444 cytokine array 7 d.p.i. *in vivo* (Figure S2), thus we conclude this does not account for the
445 electrical activity differences found during MAdV-3 acute infection. Additionally, VEGF signaling
446 activates PKC and MAPK, leading to an increase in phosphorylation of Cx43[76], however we also
447 find no significant increase in VEGF during infection *in vivo* via cytokine array. Despite this, our
448 RNA-Seq data from infected ventricular tissue are dominated by significantly increased mRNA
449 signatures of the cell-intrinsic, innate, and adaptive antiviral immune responses and we report
450 significant spleen-enlargement in infected animals (Figure 1C). Together with increased
451 macrophage infiltration during acute MAdV-3 infection (Figure 1D,E) and a detectable humoral
452 response (Figure S1F), we conclude that while the host antiviral response has been initiated
453 globally and is detectable at the mRNA level in the heart, robust cardiac inflammation has not
454 yet occurred, and the arrhythmogenic phenotypes we are observing at 7 d.p.i. herein are
455 primarily due to active viral infection rather than immune-mediated processes.
456
457 Viruses hijack cell machinery to enable their replication while hindering host cellular and
458 organismal immune responses[88,89]. Previous research has demonstrated that cGAS, a key
459 signaling molecule in the innate and cell-intrinsic interferon antiviral immune response, can pass
460 via gap junctions from infected cells to uninfected neighbors, priming and propagating the
461 antiviral state[35]. Additionally, adaptive antiviral immune responses can be amplified in this
462 manner by means of short linear peptide exchange via gap junctions effecting presentation of
463 viral antigens on HLA complexes of uninfected neighboring cells that cytotoxic CD8 T-cells can
464 engage[36]. Previously, we have reported that human adenoviral E4-ORF1 can decrease Cx43
465 protein expression through transcriptional repression via β-catenin, resulting in decreased gap
466 junction intercellular communication in human epithelial cell[38]. In addition to reduced Cx43
467 expression, we found an increase in phosphorylation of Cx43 C-terminal sites known to be
468 modified by AKT and PKC, retaining Cx43 at the cell membrane and reducing GJIC in cells
469 infected with HAdV-5[38]. In this current study, we build on these findings by investigating the

470 effects of viral modification of GJIC in the whole heart using a cardiotropic adenovirus to better
471 understand the role of infection in precipitation of the arrhythmogenic substrate.
472
473 Consistent with our prior findings, new data from HAdV-5 infected human iPSC-CMs and MAdV-
474 3 infected primary mouse cardiomyocytes *in vitro*, and MAdV-3 *in vivo* infections, reveal similar
475 induction of $Cx43^{Ser368}$ phosphorylation with concurrent reductions in gap junction function
476 (Figure 4, Figure 7). These data demonstrate a conserved mechanism between human and
477 mouse adenoviral infection occurring across diverse infected cellular populations (epithelial cells
478 and cardiomyocytes) to rapidly limit intercellular communication. Perturbed gap junction
479 coupling during adenoviral infection of the lung epithelium would presumably have limited
480 serious pathological implications for the host. Regarding infection of the working myocardium
481 however, such rapid disruptions in intercellular communication would likely precipitate
482 arrhythmias of SCD during acute infection. Our data support this scenario, whereby we find
483 $Cx43^{Ser368}$ phosphorylation occurs in concert with both uncoupling of, and altered calcium
484 handling in, iPSC-CMs *in vitro*, and decreased conduction velocity *in vivo* (Figure 3, Figure 7).
485 Critically, through implementation of mice harboring $Cx43^{S368A}$ mutation, we demonstrate that
486 phosphorylation of $Cx43^{Ser368}$ is necessary for conduction slowing we observe in MADV-3
487 infected hearts (Figure 8). Of relevance, Huke et al. previously reported a relationship between
488 reduced intercellular coupling of cardiomyocytes, the development of focal arrhythmias, and
489 increased Cx43 phosphorylation[90].
490
491 Slowed conduction velocity is a well-known arrhythmogenic determinant and is closely linked to
492 gap junction function in the heart expression[17,62,66-70]. "Previous reports have demonstrated that
493 uncoupling of cardiomyocytes favors preferential conduction velocity decrease in the
494 transverse direction of propagation This phenomenon is due to the higher gap junction
495 resistance transverse to the fiber direction[91,92]. As such, the increased spatial frequency of high
496 resistance gap junctions result in more conduction slowing transverse to fibers than along them
497 when gap junctions are inhibited[93,94]. Thus, the reductions in conduction velocity in the
498 transverse direction point to loss and/or alteration of gap junction function and can precipitate
499 arrhythmias. This propensity supports our observations of a decrease of CVT in infected mice
500 but no change in CVL as being due to gap junction dysfunction (Figure 3). We acknowledge
501 that we observe no changes in QRS interval (Figure 2D) despite significant CVT slowing
502 (Figure 3C). Discrepancy between ECG and optical measurements may be a result of the ECG
503 lacking the temporal resolution to detect differences due to His-Purkinje activation of the heart
504 in vivo, while epicardial stimulation and optical mapping slow and substantially alter activation
505 sequences such that the same effect size differences in conduction velocity and repolarization
506 can be detected.
507
508 Other viral agents have been shown to alter intercellular communication by way of
509 phosphorylation of connexins during infection. Various viruses are known to decrease
510 intercellular communication during disease, such as herpes simplex virus (HSV), feline
511 immunodeficiency virus, and bovine papillomavirus[95-97]. Herpes simplex virus type-2 infection in
512 rat liver epithelial cells increased serine phosphorylation 24 h.p.i. and reduce GJIC, resulting in
513 eventual loss of Cx43 localization at the membrane[97]. In murine fibroblasts, Rous sarcoma
514 virus, an oncogenic virus, increased phosphotyrosine and phosphoserine and reduced GJIC[98].
515 Human papillomavirus 16 (HPV16) protein E6 has been found to sequester Cx43 in the cytosol,
516 limiting trafficking and gap junction formation, and potentially facilitating tumor progression.
517 Although not directly tested, the authors report altered Cx43 phosphorylation as a likely
518 mechanism by which HPV16 E6 achieves this[99]. Additionally, a recent study found that in a
519 complex epithelia modeling of HPV infected reduced Cx43 protein and increased both protein
520 expression of Cx45 and localization at the cell membrane, and this resulted in an increase of

521 GJIC[100]. While changes to connexin phosphorylation caused by acute viral infection is most
522 commonly studied in the context of cancer biology, clearly such changes to gap junction
523 phosphorylation will also impact cardiomyocyte coupling across a variety of viral infections.
524
525 Adenoviral infection rapidly alters host-signaling cascades to facilitate viral invasion and
526 replication[101,102]. Phosphorylation of Cx43^{Ser368} is well established to occur via PKC, and we
527 confirm this in the context of adenoviral infection through implementation of two independent
528 PKC inhibitors (Figure 7A)[29,30,73-77]. Our findings of decreased conduction velocity and increased
529 Cx43^{Ser368} phosphorylation in the heart during adenovirus infection are in line with previous
530 research of the interplay between viruses and PKC signaling[103,104]. For example, early in
531 infection increased expression of adenoviral protein E1A correlates with increased PKC levels,
532 a family of kinases whose activity is required for viral endosome escape[105,106]. Adenoviral E1A is
533 the first protein expressed in the adenoviral life cycle and increased E1A correlates with
534 elevated levels of viral protein along with increased PKC protein[106]. However, the E1A activation
535 of PKC signaling in adenoviral early infection needs further delineation. PKC and downstream
536 protein signaling regulate the cell cycle, which has been well-studied in both the fields of cancer
537 and immune cell proliferation[107,108]. PKC exerts control over many cyclin genes, a particular note
538 Cyclin D, via transcription and thus can uncouple cells to start cell cycle from S phase[109].
539 Adenoviruses push cells into S phase via E1A, E1B, and E4 protein interaction with host
540 mechanisms, and this is required for viral replication[110-112]. Cardiomyocytes, themselves, are
541 typically quiescent several days after birth, and therefore, are particularly recalcitrant to entering
542 the cell cycle[113]. We must also now consider how activation of these signaling pathways shuts
543 down gap junction intercellular communication in addition to facilitating S-phase entry.
544 Therefore, acute adenoviral infection of the myocardium likely causes arrhythmogenesis via
545 activation of AKT/PKC pathways which impact Cx43, and potentially other critical cardiac ion
546 channel function.
547
548 In addition to gap junction disruption, our data provide evidence that adenoviral infection prolongs
549 action potential duration through limiting I_{K1} and I_{Ks} in adult ventricular cardiomyocytes. Ventricular
550 electrophysiology is therefore likely further compromised in addition to conduction delay in
551 infected hearts (Figure 5, Figure 6). Prolonged APD can precipitate an arrhythmogenic substrate
552 through early and/or delayed afterdepolarization in cardiomyocytes, leading to
553 tachycardia/fibrillation[114]. The APD is determined by several distinct cardiomyocyte ionic currents
554 such as sodium (I_{Na}), calcium (I_{Ca}), together with several potassium currents including I_{K1}, I_{Kr}, and
555 I_{Ks}. There is, however, a paucity of data regarding the effects of viral infection on action potential
556 duration. Turning to models of Long QT syndromes (LQT), we can interpret how alterations to
557 these currents contribute to sudden cardiac arrest. Anderson-Tawil syndrome (LQT7) is caused
558 by a monogenic defect in KCNJ2 and presents as ventricular arrhythmias, prolonged QT intervals,
559 together with physical malformations[115,116]. The ventricular arrhythmias in LQT7 are due to defects
560 in KCNJ2, the protein responsible for the Kir2.1 inward rectifier K+ current of I_{K1}, which lead to
561 spontaneous action potential durations and early/delayed afterdepolarizations[116-118]. The KCNQ1
562 and KCNE1 proteins form the K_V7.1 channel, creating the slow activating delayed rectifier current,
563 I_{Ks}[119]. Genetic modeling of LQT1 syndrome by loss-of-function in KCNQ1 causes decreased I_{Ks}
564 that underlies ventricular arrhythmias and SCD[120]. Several mutations causing LQT1 impair
565 trafficking of KCNQ1 to the cell surface, which could inform future directions in understanding the
566 effects on I_{Ks} we have identified during acute adenoviral infection[121].
567
568 Specific targeting of ion channel function has previously been described across various viral
569 species and host cell types. In a cardiac model, CVB3 viral titers were increased in the *mayday*
570 mutant mouse model; these mice are deficient in Kir6.1, a subunit of KATP channels, and had
571 decreased survivability after infection[122,123]. Turning to non-cardiac excitable tissues, patch

572 clamping experiments of neuroblastoma cells that were infected with rabies virus displayed
573 decreased I_{Kir} and I_{Na} amplitude 3 d.p.i with no observable morphological changes[124]. While
574 many of these studies lack a viral mechanistic cause of the change in K+ currents, it is plausible
575 to consider this as a viral advantage, as viruses across different realms clearly and specifically
576 alter such ionic currents during infection. Potassium channels are ubiquitously found across
577 almost all cell types, including non-excitable cells. This included the epithelium, a common entry
578 point for most viruses, and other cell types such as immune cells, such as macrophages and T-
579 cells[125-128]. Interestingly, K+ channels in the epithelium are localized along the basolateral
580 membrane, coincident with the Coxsackie adenovirus receptor (CAR) and integrins utilized by
581 human adenoviruses for entry[126].
582
583 It is conceivable that a common mechanism underlies the arrhythmogenic alterations to gap
584 junctions and K+ currents we report. PKC is known to phosphorylate a multitude of host proteins
585 relevant to our findings, including K_V7.1 and Cx43[31]. As the kinase responsible for
586 phosphorylation of Cx43^{Ser368}, PKC activation is well-described in subsequent reduced gap
587 junction channel opening probability[29,30,129]. PKC signaling is also known to regulate I_{Ks} by
588 promoting K_V7.1 endocytosis through increased phosphorylation of KCNE1[31]. When broadly
589 looking at the role of kinases during ischemic stress and heart failure, PKC signaling has been
590 found to be sufficient in I_{K1} reduction[130]. The commonality between negative regulation of Cx43
591 and I_{K1} and I_{Ks} currents by PKC strongly implicates it as a potential central kinase activated
592 during viral infection that concurrently, and dangerously, affects distinct arms of cardiac
593 electrophysiology. Given that PKC isoforms are known to regulate many endosomal functions,
594 such as endocytosis and trafficking from the membrane, it is unsurprising that many viruses
595 target this pathway for host cell invasion[131]. The direct interaction with PKC family members is
596 vital for influenza assembly, replication machinery function, and endosomal exit[132,133]. For
597 example, West Nile virus replication is inhibited when PKC activity is blocked and viral fusion of
598 Respiratory Syncytial Virus (RSV) requires PKCα membrane translocation[103,134]. Thus,
599 modification of the PKC family is a common mechanistic target across viral families.
600
601 The question remains as to how and why a DNA tumor virus such as adenovirus would infect
602 terminally differentiated muscle, such as the working myocardium. As mentioned above,
603 adenoviruses induce cell cycle entry to facilitate their own genome replication by arresting
604 infected cells in S-phase[46]. Given their recalcitrance to cell cycle entry, compared to epithelial
605 cells, it is tempting to speculate that adult cardiomyocytes are not the intended host cell for
606 adenovirus, but when infected, precipitate an unfortunate and potentially deadly pathological
607 process. Human adenoviruses are understood to primarily utilize CAR for binding and host cell
608 entry, just like CVB3, although CAR-independent infection is also reported[61,135-137]. A component
609 of the intercellular junction, CAR is expressed in several tissue types, including the heart, where
610 it is primarily expressed on endothelial, epithelial cells, and at the cardiomyocyte ID[138,139]. In
611 cardiomyocytes, CAR appears to play an integral role in coupling cells together for
612 electromechanical and metabolic signaling[140,141]. The enrichment of CAR in the heart may, in
613 part, contribute to adenoviral infection and colonization of this tissue should viremia occur, for
614 example.
615
616 Aside from the significant body of viral myocarditis research employing CVB3, reovirus has also
617 been developed as a model which, while typically not causing disease in humans, elicits
618 myocarditis in neonatal mice[142]. Acute reovirus infection causes cytopathic effect specifically in
619 cardiomyocytes, as compared to fibroblasts or epithelial cells[143]. This increases inflammation
620 and infiltration of host immune cells, which is a common pathogenesis to that reported in CVB3
621 infection[144]. Mouse adenovirus Type-1 (MAdV-1) has previously been employed to investigate
622 adenoviral-specific cardiac infection. The Weinberg group has shown significant inflammation of

623 cardiac tissue and immune cell infiltration during chronic MAdV-1 infection[56,57]. During MAdV-1
624 infection, the progression of myocardial inflammation *in vivo* was assessed and viral loads in the
625 heart peak between 7-10 d.p.i., but consistent with our findings at 7 d.p.i. with MAdV-3 (Figure
626 1E), significant inflammation by CD3+ cell count and cardiac troponin I serum levels were not
627 detected until 10 d.p.i.[56]. This MAdV-1 response occurred along with high levels of IFN-γ, and
628 the immunoproteasome induced in a dose-dependent and inverse age-dependent manner that
629 followed IFN-γ levels[56,57,145]. These models are beneficial to understand the role of direct and
630 indirect immune-mediated responses in the heart during infection with a virus that also afflicts
631 the respiratory system[146]. Together, while this research has contributed much to our
632 understanding of viral-mediated inflammation of the heart, previous studies demonstrate that
633 there are pathogen-specific effects to the host cell at the molecular level, especially relevant to
634 acute stages of myocarditis[83].
635
636 In order to consistently induce MAdV-3 cardiac infection through induction of a reproducible
637 viremia or controlled inoculum we employed the retro-orbital route of administration. While this
638 differs from natural mechanisms preceding adenoviral myocarditis (such as infection of the gut
639 or lung for example, prior to viremia and subsequent viremia and cardiac infection) our goals
640 were to focus solely on pathological mechanisms in cardiac tissue once infected. Introduction of
641 a consistent inoculum in this manner was necessary, ensuring similar exposure of cardiac
642 muscle to virus while avoiding variability of viremia induction through other routes of
643 administration. Having established that direct viral infection can precipitate dangerous
644 electrophysiological remodeling in the heart, our findings provide groundwork for future studies
645 investigating mechanisms of adenoviral cardiotropism, including why certain groups may be
646 susceptible.
647
648 As acute infections are hypothesized to be a significant cause of sudden cardiac arrest, we
649 sought to employ MAdV-3 as a novel acute adenoviral myocarditis model. Through studying the
650 infected heart at early stages of viral colonization and replication, we have revealed previously
651 underappreciated effects of viral-mediated changes to cardiomyocytes precipitating
652 electrophysiological defects and leading to an arrhythmogenic substrate. Overall, there has
653 been a paucity of research into direct adenoviral mechanisms that induce arrhythmogenesis and
654 our data introduce MAdV-3 infection as a viable model with which to study adenoviral cardiac
655 infection and myocarditis progression in the adult mouse. Relevance to human disease is
656 confirmed through complementary work in HiPSC-CMs and HAdV-5 where we find infected
657 cardiomyocytes undergo arrhythmogenic alterations to intercellular coupling and
658 electrophysiology while still viable, and in the absence of an inflammatory or adaptive host
659 immune system. Clinical relevance is also confirmed through our *in vivo* studies where, just as
660 in human patients, we uncover an arrhythmogenic substrate in infected hearts which are free of
661 any remarkable cardiomyopathy or inflammation[8]. Truly parsing out viral effects independent of
662 the host inflammatory response is not possible, however, and contributions of inflammatory
663 cytokines to our *in vivo* observations must be considered. Implementation of models to
664 limit/modulate host immune responses may be somewhat informative here but given that in
665 such immunocompromised contexts, viral replication and spread would be artifactually
666 augmented, and physiologically relevance compromised. Overall, our data provide insight not
667 just into mechanisms of arrhythmogenesis during acute cardiac adenoviral infection, but also
668 the state of key players in cardiac electrophysiology in phases of disease preceding gross
669 remodeling of myocarditis and progression to heart failure. In addition to informing therapeutic
670 interventions, the ability to model acute cardiac infection will facilitate development of diagnostic
671 approaches to identify at-risk individuals with limited clinical presentation by current
672 screening/imaging methods. **Acknowledgments**

The authors thank Dr. Allison N. Tegge (Department of Statistics, Virginia Tech) for assisting in statistical analyses and design and Dr. Sarah Barrett (Virginia-Maryland College of Veterinary Medicine) for undertaking histopathology. The authors also thank Eric Sapp, Alex Ix, and Kenneth Young II for technical support. This work was supported by NIH NHLBI R01 grants: HL132236 and HL159512 to J.W.S.; HL138003 and HL141855 to S.P., NINDS R01 grant NS105804 and R21 grant NS128635 to S.A.S., NHLBI R35 grant HL161237P to R.G.G., NHLBI F31 grants: HL152649 to R.L.P.; HL160172 to G.A.B.; HL147438 to D.R.K., American Heart Association predoctoral fellowship award 23PRE1025476 to K.E.S., FBRI Seale Innovation Award to J.W.S., and a FBRI Lyerly Postdoctoral Excellence Award to C.M.P..

Author contributions

J.W.S. and R.L.P. designed this study. R.L.P. performed cell and animal infections, viral propagation, primary cell isolations, RT-qPCR, qPCR, confocal immunofluorescence microscopy, western blotting, troponin ELISA, live cell imagining, echocardiography experiments and analysis. M.J.Z. analyzed RNA-Seq data, performed RT-qPCR, qPCR, confocal, western blotting, differentiated and cultured HiPSC-CMs, and assisted in all data analyses and statistics. G.A.B. and X.W. performed the optical mapping and analysis. M.T.T. performed and analyzed the echocardiograms. M.D.N. and K.E.S. performed *in vivo* infections, cryosectioning, and confocal immunofluorescence microscopy with analyses. C.M.P. performed RNA-Seq analysis and confocal immunofluorescence microscopy with analyses. S.L. performed humoral immune response ELISA as well as biochemistry and western blotting. R.G.G. provided input on optical mapping experimental design and manuscript feedback. D.R.K. and G.S.H. assisted in design and analysis of optical mapping and electrophysiology experiments. S.A.S. performed and analyzed the patch clamping experiments. S.P. provided optical mapping and electrophysiology experimental design, data analysis, and manuscript feedback. J.W.S. supervised all work and performed the cytokine array, primary cardiomyocyte isolations, and live cell imaging analysis. J.W.S., R.L.P., and M.J.Z. analyzed the data and interpretation. R.L.P. wrote the manuscript with J.W.S. with input from M.J.Z.

Declaration of interests

The authors declare no competing interests.

Supplemental Materials

Expanded Materials and Methods
Online Figures S1-S4 and Legends
Online Videos S1 and S2
Major Resources Table
References 62-79

712 **References**
713
714 1. Babu-Narayan SV, McCarthy KP, Ho SY, Magee AG, Kilner PJ, Sheppard MN. Images
715 in cardiovascular medicine. Myocarditis and sudden cardiac death in the young:
716 extensive fibrosis suggested by cardiovascular magnetic resonance in vivo and
717 confirmed post mortem. Circulation. 2007;116:e122-125. doi:
718 10.1161/CIRCULATIONAHA.107.693085
719 2. Dennert R, Crijns HJ, Heymans S. Acute viral myocarditis. Eur Heart J. 2008;29:2073-
720 2082. doi: 10.1093/eurheartj/ehn296
721 3. Baksi AJ, Kanaganayagam GS, Prasad SK. Arrhythmias in viral myocarditis and
722 pericarditis. Card Electrophysiol Clin. 2015;7:269-281. doi: 10.1016/j.ccep.2015.03.009
723 4. Woodruff JF. Viral myocarditis. A review. The American journal of pathology.
724 1980;101:425-484.
725 5. Blauwet LA, Cooper LT. Myocarditis. Prog Cardiovasc Dis. 2010;52:274-288. doi:
726 10.1016/j.pcad.2009.11.006
727 6. Kuhl U, Pauschinger M, Seeberg B, Lassner D, Noutsias M, Poller W, Schultheiss HP.
728 Viral persistence in the myocardium is associated with progressive cardiac dysfunction.
729 Circulation. 2005;112:1965-1970. doi: 10.1161/CIRCULATIONAHA.105.548156
730 7. Tschope C, Ammirati E, Bozkurt B, Caforio ALP, Cooper LT, Felix SB, Hare JM,
731 Heidecker B, Heymans S, Hubner N, et al. Myocarditis and inflammatory
732 cardiomyopathy: current evidence and future directions. Nat Rev Cardiol. 2021;18:169-
733 193. doi: 10.1038/s41569-020-00435-x
734 8. Ammirati E, Cipriani M, Moro C, Raineri C, Pini D, Sormani P, Mantovani R, Varrenti M,
735 Pedrotti P, Conca C, et al. Clinical Presentation and Outcome in a Contemporary Cohort
736 of Patients With Acute Myocarditis: Multicenter Lombardy Registry. Circulation.
737 2018;138:1088-1099. doi: 10.1161/CIRCULATIONAHA.118.035319
738 9. Leoni D, Rello J. Cardiac arrest among patients with infections: causes, clinical practice
739 and research implications. Clin Microbiol Infect. 2017;23:730-735. doi:
740 10.1016/j.cmi.2016.11.018
741 10. Harris KM, Mackey-Bojack S, Bennett M, Nwaudo D, Duncanson E, Maron BJ. Sudden
742 Unexpected Death Due to Myocarditis in Young People, Including Athletes. Am J
743 Cardiol. 2021;143:131-134. doi: 10.1016/j.amjcard.2020.12.028
744 11. Liberthson RR. Sudden death from cardiac causes in children and young adults. N Engl
745 J Med. 1996;334:1039-1044. doi: 10.1056/NEJM199604183341607
746 12. Grant AO. Cardiac ion channels. Circ Arrhythm Electrophysiol. 2009;2:185-194. doi:
747 10.1161/CIRCEP.108.789081
748 13. Kurtenbach S, Kurtenbach S, Zoidl G. Gap junction modulation and its implications for
749 heart function. Front Physiol. 2014;5:82. doi: 10.3389/fphys.2014.00082
750 14. Smyth JW, Shaw RM. The gap junction life cycle. Heart Rhythm. 2012;9:151-153. doi:
751 10.1016/j.hrthm.2011.07.028
752 15. Nattel S, Maguy A, Le Bouter S, Yeh YH. Arrhythmogenic ion-channel remodeling in the
753 heart: heart failure, myocardial infarction, and atrial fibrillation. Physiological reviews.
754 2007;87:425-456. doi: 10.1152/physrev.00014.2006
755 16. Kucera JP, Rohr S, Rudy Y. Localization of sodium channels in intercalated disks
756 modulates cardiac conduction. Circulation research. 2002;91:1176-1182. doi:
757 10.1161/01.res.0000046237.54156.0a
758 17. Rohr S. Role of gap junctions in the propagation of the cardiac action potential.
759 Cardiovascular research. 2004;62:309-322. doi: 10.1016/j.cardiores.2003.11.035
760 18. Noutsias M, Fechner H, de Jonge H, Wang X, Dekkers D, Houtsmuller AB, Pauschinger
761 M, Bergelson J, Warraich R, Yacoub M, et al. Human coxsackie-adenovirus receptor is
762 colocalized with integrins alpha(v)beta(3) and alpha(v)beta(5) on the cardiomyocyte

763 sarcolemma and upregulated in dilated cardiomyopathy: implications for cardiotropic
764 viral infections. Circulation. 2001;104:275-280. doi: 10.1161/01.cir.104.3.275
765 19. Veeraraghavan R, Hoeker GS, Alvarez-Laviada A, Hoagland D, Wan X, King DR,
766 Sanchez-Alonso J, Chen C, Jourdan J, Isom LL, et al. The adhesion function of the
767 sodium channel beta subunit (beta1) contributes to cardiac action potential propagation.
768 Elife. 2018;7. doi: 10.7554/eLife.37610
769 20. George SA, Hoeker G, Calhoun PJ, Entz M, 2nd, Raisch TB, King DR, Khan M, Baker
770 C, Gourdie RG, Smyth JW, et al. Modulating cardiac conduction during metabolic
771 ischemia with perfusate sodium and calcium in guinea pig hearts. American journal of
772 physiology Heart and circulatory physiology. 2019;316:H849-H861. doi:
773 10.1152/ajpheart.00083.2018
774 21. Agullo-Pascual E, Lin X, Leo-Macias A, Zhang M, Liang FX, Li Z, Pfenniger A,
775 Lubkemeier I, Keegan S, Fenyo D, et al. Super-resolution imaging reveals that loss of
776 the C-terminus of connexin43 limits microtubule plus-end capture and NaV1.5
777 localization at the intercalated disc. Cardiovascular research. 2014;104:371-381. doi:
778 10.1093/cvr/cvu195
779 22. Vermij SH, Abriel H, van Veen TA. Refining the molecular organization of the cardiac
780 intercalated disc. Cardiovascular research. 2017;113:259-275. doi: 10.1093/cvr/cvw259
781 23. Palatinus JA, O'Quinn MP, Barker RJ, Harris BS, Jourdan J, Gourdie RG. ZO-1
782 determines adherens and gap junction localization at intercalated disks. American
783 journal of physiology Heart and circulatory physiology. 2011;300:H583-594. doi:
784 10.1152/ajpheart.00999.2010
785 24. Chkourko HS, Guerrero-Serna G, Lin X, Darwish N, Pohlmann JR, Cook KE, Martens
786 JR, Rothenberg E, Musa H, Delmar M. Remodeling of mechanical junctions and of
787 microtubule-associated proteins accompany cardiac connexin43 lateralization. Heart
788 Rhythm. 2012;9:1133-1140 e1136. doi: 10.1016/j.hrthm.2012.03.003
789 25. Peters NS, Coromilas J, Severs NJ, Wit AL. Disturbed connexin43 gap junction
790 distribution correlates with the location of reentrant circuits in the epicardial border zone
791 of healing canine infarcts that cause ventricular tachycardia. Circulation. 1997;95:988-
792 996.
793 26. Smyth JW, Hong TT, Gao D, Vogan JM, Jensen BC, Fong TS, Simpson PC, Stainier
794 DY, Chi NC, Shaw RM. Limited forward trafficking of connexin 43 reduces cell-cell
795 coupling in stressed human and mouse myocardium. The Journal of clinical
796 investigation. 2010;120:266-279. doi: 10.1172/JCI39740
797 27. Yajima T, Knowlton KU. Viral myocarditis: from the perspective of the virus. Circulation.
798 2009;119:2615-2624. doi: 10.1161/CIRCULATIONAHA.108.766022
799 28. Lei M, Xu J, Gao Q, Minobe E, Kameyama M, Hao L. PKA phosphorylation of Cav1.2
800 channel modulates the interaction of calmodulin with the C terminal tail of the channel. J
801 Pharmacol Sci. 2018;137:187-194. doi: 10.1016/j.jphs.2018.05.010
802 29. Lampe PD, TenBroek EM, Burt JM, Kurata WE, Johnson RG, Lau AF. Phosphorylation
803 of connexin43 on serine368 by protein kinase C regulates gap junctional communication.
804 The Journal of cell biology. 2000;149:1503-1512.
805 30. Ek-Vitorin JF, King TJ, Heyman NS, Lampe PD, Burt JM. Selectivity of connexin 43
806 channels is regulated through protein kinase C-dependent phosphorylation. Circulation
807 research. 2006;98:1498-1505. doi: 10.1161/01.RES.0000227572.45891.2c
808 31. Kanda VA, Purtell K, Abbott GW. Protein kinase C downregulates I(Ks) by stimulating
809 KCNQ1-KCNE1 potassium channel endocytosis. Heart Rhythm. 2011;8:1641-1647. doi:
810 10.1016/j.hrthm.2011.04.034
811 32. Jiang M, Xu X, Wang Y, Toyoda F, Liu XS, Zhang M, Robinson RB, Tseng GN. Dynamic
812 partnership between KCNQ1 and KCNE1 and influence on cardiac IKs current amplitude

813 by KCNE2. The Journal of biological chemistry. 2009;284:16452-16462. doi:
814 10.1074/jbc.M808262200
815 33. Jongsma HJ, Wilders R. Gap junctions in cardiovascular disease. Circulation research.
816 2000;86:1193-1197.
817 34. Vozzi C, Dupont E, Coppen SR, Yeh HI, Severs NJ. Chamber-related differences in
818 connexin expression in the human heart. Journal of molecular and cellular cardiology.
819 1999;31:991-1003. doi: 10.1006/jmcc.1999.0937
820 35. Ablasser A, Schmid-Burgk JL, Hemmerling I, Horvath GL, Schmidt T, Latz E, Hornung V.
821 Cell intrinsic immunity spreads to bystander cells via the intercellular transfer of cGAMP.
822 Nature. 2013;503:530-534. doi: 10.1038/nature12640
823 36. Neijssen J, Herberts C, Drijfhout JW, Reits E, Janssen L, Neefjes J. Cross-presentation
824 by intercellular peptide transfer through gap junctions. Nature. 2005;434:83-88. doi:
825 10.1038/nature03290
826 37. Patel SJ, King KR, Casali M, Yarmush ML. DNA-triggered innate immune responses are
827 propagated by gap junction communication. Proceedings of the National Academy of
828 Sciences of the United States of America. 2009;106:12867-12872. doi:
829 10.1073/pnas.0809292106
830 38. Calhoun PJ, Phan AV, Taylor JD, James CC, Padget RL, Zeitz MJ, Smyth JW.
831 Adenovirus targets transcriptional and posttranslational mechanisms to limit gap junction
832 function. FASEB J. 2020;34:9694-9712. doi: 10.1096/fj.202000667R
833 39. Shauer A, Gotsman I, Keren A, Zwas DR, Hellman Y, Durst R, Admon D. Acute viral
834 myocarditis: current concepts in diagnosis and treatment. Isr Med Assoc J. 2013;15:180-
835 185.
836 40. Escher F, Pietsch H, Aleshcheva G, Bock T, Baumeier C, Elsaesser A, Wenzel P,
837 Hamm C, Westenfeld R, Schultheiss M, et al. Detection of viral SARS-CoV-2 genomes
838 and histopathological changes in endomyocardial biopsies. ESC Heart Fail.
839 2020;7:2440-2447. doi: 10.1002/ehf2.12805
840 41. Shah KS, Hale Hammond ME, Drakos SG, Anderson JL, Fang JC, Knowlton KU, Shaw
841 RM. SARS-CoV-2 as an inflammatory cardiovascular disease: current knowledge and
842 future challenges. Future Cardiol. 2021;17:1277-1291. doi: 10.2217/fca-2020-0188
843 42. Garmaroudi FS, Marchant D, Hendry R, Luo H, Yang D, Ye X, Shi J, McManus BM.
844 Coxsackievirus B3 replication and pathogenesis. Future Microbiol. 2015;10:629-653. doi:
845 10.2217/fmb.15.5
846 43. Knowlton KU. CVB infection and mechanisms of viral cardiomyopathy. Curr Top
847 Microbiol Immunol. 2008;323:315-335.
848 44. Lim BK, Peter AK, Xiong D, Narezkina A, Yung A, Dalton ND, Hwang KK, Yajima T,
849 Chen J, Knowlton KU. Inhibition of Coxsackievirus-associated dystrophin cleavage
850 prevents cardiomyopathy. The Journal of clinical investigation. 2013;123:5146-5151. doi:
851 10.1172/JCI66271
852 45. Nagy PD, Pogany J. The dependence of viral RNA replication on co-opted host factors.
853 Nat Rev Microbiol. 2011;10:137-149. doi: 10.1038/nrmicro2692
854 46. O'Shea CC. DNA tumor viruses -- the spies who lyse us. Curr Opin Genet Dev.
855 2005;15:18-26. doi: 10.1016/j.gde.2004.12.010
856 47. Greber UF. Adenoviruses - Infection, pathogenesis and therapy. FEBS letters.
857 2020;594:1818-1827. doi: 10.1002/1873-3468.13849
858 48. Schneider-Schaulies J. Cellular receptors for viruses: links to tropism and pathogenesis.
859 J Gen Virol. 2000;81:1413-1429. doi: 10.1099/0022-1317-81-6-1413
860 49. Pauschinger M, Bowles NE, Fuentes-Garcia FJ, Pham V, Kuhl U, Schwimmbeck PL,
861 Schultheiss HP, Towbin JA. Detection of adenoviral genome in the myocardium of adult
862 patients with idiopathic left ventricular dysfunction. Circulation. 1999;99:1348-1354. doi:
863 10.1161/01.cir.99.10.1348

50. Treacy A, Carr MJ, Dunford L, Palacios G, Cannon GA, O'Grady A, Moran J, Hassan J, Loy A, Connell J, et al. First report of sudden death due to myocarditis caused by adenovirus serotype 3. J Clin Microbiol. 2010;48:642-645. doi: 10.1128/JCM.00815-09
51. Bowles NE, Ni J, Kearney DL, Pauschinger M, Schultheiss HP, McCarthy R, Hare J, Bricker JT, Bowles KR, Towbin JA. Detection of viruses in myocardial tissues by polymerase chain reaction. evidence of adenovirus as a common cause of myocarditis in children and adults. J Am Coll Cardiol. 2003;42:466-472.
52. O'Shea CC, Choi S, McCormick F, Stokoe D. Adenovirus overrides cellular checkpoints for protein translation. Cell Cycle. 2005;4:883-888.
53. Turner RL, Groitl P, Dobner T, Ornelles DA. Adenovirus replaces mitotic checkpoint controls. J Virol. 2015;89:5083-5096. doi: 10.1128/JVI.00213-15
54. Smyth JW, Zhang SS, Sanchez JM, Lamouille S, Vogan JM, Hesketh GG, Hong T, Tomaselli GF, Shaw RM. A 14-3-3 mode-1 binding motif initiates gap junction internalization during acute cardiac ischemia. Traffic. 2014;15:684-699. doi: 10.1111/tra.12169
55. Bertzbach LD, Ip WH, Dobner T. Animal Models in Human Adenovirus Research. Biology (Basel). 2021;10. doi: 10.3390/biology10121253
56. McCarthy MK, Procario MC, Twisselmann N, Wilkinson JE, Archambeau AJ, Michele DE, Day SM, Weinberg JB. Proinflammatory effects of interferon gamma in mouse adenovirus 1 myocarditis. J Virol. 2015;89:468-479. doi: 10.1128/JVI.02077-14
57. Chandrasekaran A, Adkins LJ, Seltzer HM, Pant K, Tryban ST, Molloy CT, Weinberg JB. Age-Dependent Effects of Immunoproteasome Deficiency on Mouse Adenovirus Type 1 Pathogenesis. J Virol. 2019;93. doi: 10.1128/JVI.00569-19
58. Weinberg JB, Stempfle GS, Wilkinson JE, Younger JG, Spindler KR. Acute respiratory infection with mouse adenovirus type 1. Virology. 2005;340:245-254. doi: 10.1016/j.virol.2005.06.021
59. Gralinski LE, Ashley SL, Dixon SD, Spindler KR. Mouse adenovirus type 1-induced breakdown of the blood-brain barrier. J Virol. 2009;83:9398-9410. doi: 10.1128/JVI.00954-09
60. Klempa B, Kruger DH, Auste B, Stanko M, Krawczyk A, Nickel KF, Uberla K, Stang A. A novel cardiotropic murine adenovirus representing a distinct species of mastadenoviruses. J Virol. 2009;83:5749-5759. doi: 10.1128/JVI.02281-08
61. Bieri M, Hendrickx R, Bauer M, Yu B, Jetzer T, Dreier B, Mittl PRE, Sobek J, Pluckthun A, Greber UF, et al. The RGD-binding integrins alphavbeta6 and alphavbeta8 are receptors for mouse adenovirus-1 and -3 infection. PLoS Pathog. 2021;17:e1010083. doi: 10.1371/journal.ppat.1010083
62. Huang GY, Xie LJ, Linask KL, Zhang C, Zhao XQ, Yang Y, Zhou GM, Wu YJ, Marquez-Rosado L, McElhinney DB, et al. Evaluating the role of connexin43 in congenital heart disease: Screening for mutations in patients with outflow tract anomalies and the analysis of knock-in mouse models. J Cardiovasc Dis Res. 2011;2:206-212. doi: 10.4103/0975-3583.89804
63. Smyth JW, Vogan JM, Buch PJ, Zhang SS, Fong TS, Hong TT, Shaw RM. Actin cytoskeleton rest stops regulate anterograde traffic of connexin 43 vesicles to the plasma membrane. Circulation research. 2012;110:978-989. doi: 10.1161/CIRCRESAHA.111.257964
64. Burridge PW, Holmstrom A, Wu JC. Chemically Defined Culture and Cardiomyocyte Differentiation of Human Pluripotent Stem Cells. Curr Protoc Hum Genet. 2015;87:21 23 21-21 23 15. doi: 10.1002/0471142905.hg2103s87
65. Burridge PW, Matsa E, Shukla P, Lin ZC, Churko JM, Ebert AD, Lan F, Diecke S, Huber B, Mordwinkin NM, et al. Chemically defined generation of human cardiomyocytes. Nat Methods. 2014;11:855-860. doi: 10.1038/nmeth.2999

66. Buikema JW, Lee S, Goodyer WR, Maas RG, Chirikian O, Li G, Miao Y, Paige SL, Lee D, Wu H, et al. Wnt Activation and Reduced Cell-Cell Contact Synergistically Induce Massive Expansion of Functional Human iPSC-Derived Cardiomyocytes. Cell Stem Cell. 2020;27:50-63 e55. doi: 10.1016/j.stem.2020.06.001
67. Feyen DAM, McKeithan WL, Bruyneel AAN, Spiering S, Hormann L, Ulmer B, Zhang H, Briganti F, Schweizer M, Hegyi B, et al. Metabolic Maturation Media Improve Physiological Function of Human iPSC-Derived Cardiomyocytes. Cell reports. 2020;32:107925. doi: 10.1016/j.celrep.2020.107925
68. Green M, Loewenstein PM. Human adenoviruses: propagation, purification, quantification, and storage. Curr Protoc Microbiol. 2006;Chapter 14:Unit 14C 11. doi: 10.1002/9780471729259.mc14c01s00
69. O'Connell TD, Rodrigo MC, Simpson PC. Isolation and culture of adult mouse cardiac myocytes. Methods in molecular biology. 2007;357:271-296. doi: 10.1385/1-59745-214-9:271
70. Fernandez NF, Gundersen GW, Rahman A, Grimes ML, Rikova K, Hornbeck P, Ma'ayan A. Clustergrammer, a web-based heatmap visualization and analysis tool for high-dimensional biological data. Sci Data. 2017;4:170151. doi: 10.1038/sdata.2017.151
71. Wu T, Hu E, Xu S, Chen M, Guo P, Dai Z, Feng T, Zhou L, Tang W, Zhan L, et al. clusterProfiler 4.0: A universal enrichment tool for interpreting omics data. Innovation (Camb). 2021;2:100141. doi: 10.1016/j.xinn.2021.100141
72. Smyth JW, Fleeton MN, Sheahan BJ, Atkins GJ. Treatment of rapidly growing K-BALB and CT26 mouse tumours using Semliki Forest virus and its derived vector. Gene Ther. 2005;12:147-159. doi: 10.1038/sj.gt.3302390
73. Lindsey ML, Escobar GP, Mukherjee R, Goshorn DK, Sheats NJ, Bruce JA, Mains IM, Hendrick JK, Hewett KW, Gourdie RG, et al. Matrix metalloproteinase-7 affects connexin-43 levels, electrical conduction, and survival after myocardial infarction. Circulation. 2006;113:2919-2928. doi: 10.1161/CIRCULATIONAHA.106.612960
74. George SA, Sciuto KJ, Lin J, Salama ME, Keener JP, Gourdie RG, Poelzing S. Extracellular sodium and potassium levels modulate cardiac conduction in mice heterozygous null for the Connexin43 gene. Pflugers Arch. 2015;467:2287-2297. doi: 10.1007/s00424-015-1698-0
75. King DR, Entz M, 2nd, Blair GA, Crandell I, Hanlon AL, Lin J, Hoeker GS, Poelzing S. The conduction velocity-potassium relationship in the heart is modulated by sodium and calcium. Pflugers Arch. 2021;473:557-571. doi: 10.1007/s00424-021-02537-y
76. Smyth JW, Shaw RM. Autoregulation of connexin43 gap junction formation by internally translated isoforms. Cell reports. 2013;5:611-618. doi: 10.1016/j.celrep.2013.10.009
77. Zeitz MJ, Calhoun PJ, James CC, Taetzsch T, George KK, Robel S, Valdez G, Smyth JW. Dynamic UTR Usage Regulates Alternative Translation to Modulate Gap Junction Formation during Stress and Aging. Cell reports. 2019;27:2737-2747 e2735. doi: 10.1016/j.celrep.2019.04.114
78. Schindelin J, Arganda-Carreras I, Frise E, Kaynig V, Longair M, Pietzsch T, Preibisch S, Rueden C, Saalfeld S, Schmid B, et al. Fiji: an open-source platform for biological-image analysis. Nat Methods. 2012;9:676-682. doi: 10.1038/nmeth.2019
79. Walter A, Saric T, Hescheler J, Papadopoulos S. Calcium Imaging in Pluripotent Stem Cell-Derived Cardiac Myocytes. Methods in molecular biology. 2016;1353:131-146. doi: 10.1007/7651_2015_267
80. Shaw RM, Rudy Y. Ionic mechanisms of propagation in cardiac tissue. Roles of the sodium and L-type calcium currents during reduced excitability and decreased gap junction coupling. Circulation research. 1997;81:727-741.

964 81. Veeraraghavan R, Lin J, Hoeker GS, Keener JP, Gourdie RG, Poelzing S. Sodium
965 channels in the Cx43 gap junction perinexus may constitute a cardiac ephapse: an
966 experimental and modeling study. Pflugers Arch. 2015. doi: 10.1007/s00424-014-1675-z
967 82. Kirchhoff S, Nelles E, Hagendorff A, Kruger O, Traub O, Willecke K. Reduced cardiac
968 conduction velocity and predisposition to arrhythmias in connexin40-deficient mice. Curr
969 Biol. 1998;8:299-302. doi: 10.1016/s0960-9822(98)70114-9
970 83. Aronis KN, Ali RL, Prakosa A, Ashikaga H, Berger RD, Hakim JB, Liang J, Tandri H,
971 Teng F, Chrispin J, et al. Accurate Conduction Velocity Maps and Their Association With
972 Scar Distribution on Magnetic Resonance Imaging in Patients With Postinfarction
973 Ventricular Tachycardias. Circ Arrhythm Electrophysiol. 2020;13:e007792. doi:
974 10.1161/CIRCEP.119.007792
975 84. Akar FG, Nass RD, Hahn S, Cingolani E, Shah M, Hesketh GG, DiSilvestre D, Tunin RS,
976 Kass DA, Tomaselli GF. Dynamic changes in conduction velocity and gap junction
977 properties during development of pacing-induced heart failure. American journal of
978 physiology Heart and circulatory physiology. 2007;293:H1223-1230. doi:
979 10.1152/ajpheart.00079.2007
980 85. Poelzing S, Rosenbaum DS. Altered connexin43 expression produces arrhythmia
981 substrate in heart failure. American journal of physiology Heart and circulatory
982 physiology. 2004;287:H1762-1770. doi: 10.1152/ajpheart.00346.2004
983 86. Akar FG, Spragg DD, Tunin RS, Kass DA, Tomaselli GF. Mechanisms underlying
984 conduction slowing and arrhythmogenesis in nonischemic dilated cardiomyopathy.
985 Circulation research. 2004;95:717-725. doi: 10.1161/01.RES.0000144125.61927.1c
986 87. Cone AC, Cavin G, Ambrosi C, Hakozaki H, Wu-Zhang AX, Kunkel MT, Newton AC,
987 Sosinsky GE. Protein kinase Cdelta-mediated phosphorylation of Connexin43 gap
988 junction channels causes movement within gap junctions followed by vesicle
989 internalization and protein degradation. The Journal of biological chemistry.
990 2014;289:8781-8798. doi: 10.1074/jbc.M113.533265
991 88. Fong JT, Nimlamool W, Falk MM. EGF induces efficient Cx43 gap junction endocytosis
992 in mouse embryonic stem cell colonies via phosphorylation of Ser262, Ser279/282, and
993 Ser368. FEBS letters. 2014;588:836-844. doi: 10.1016/j.febslet.2014.01.048
994 89. Lastwika KJ, Dunn CA, Solan JL, Lampe PD. Phosphorylation of connexin 43 at MAPK,
995 PKC or CK1 sites each distinctly alter the kinetics of epidermal wound repair. Journal of
996 cell science. 2019;132. doi: 10.1242/jcs.234633
997 90. Nimlamool W, Andrews RM, Falk MM. Connexin43 phosphorylation by PKC and MAPK
998 signals VEGF-mediated gap junction internalization. Molecular biology of the cell.
999 2015;26:2755-2768. doi: 10.1091/mbc.E14-06-1105
1000 91. Richards TS, Dunn CA, Carter WG, Usui ML, Olerud JE, Lampe PD. Protein kinase C
1001 spatially and temporally regulates gap junctional communication during human wound
1002 repair via phosphorylation of connexin43 on serine368. The Journal of cell biology.
1003 2004;167:555-562. doi: 10.1083/jcb.200404142
1004 92. Evenou JP, Wagner J, Zenke G, Brinkmann V, Wagner K, Kovarik J, Welzenbach KA,
1005 Weitz-Schmidt G, Guntermann C, Towbin H, et al. The potent protein kinase C-selective
1006 inhibitor AEB071 (sotrastaurin) represents a new class of immunosuppressive agents
1007 affecting early T-cell activation. J Pharmacol Exp Ther. 2009;330:792-801. doi:
1008 10.1124/jpet.109.153205
1009 93. Wagner J, von Matt P, Sedrani R, Albert R, Cooke N, Ehrhardt C, Geiser M, Rummel G,
1010 Stark W, Strauss A, et al. Discovery of 3-(1H-indol-3-yl)-4-[2-(4-methylpiperazin-1-
1011 yl)quinazolin-4-yl]pyrrole-2,5-dione (AEB071), a potent and selective inhibitor of protein
1012 kinase C isotypes. J Med Chem. 2009;52:6193-6196. doi: 10.1021/jm901108b

1013 94. Dieter P, Fitzke E. RO 31-8220 and RO 31-7549 show improved selectivity for protein
1014 kinase C over staurosporine in macrophages. Biochemical and biophysical research
1015 communications. 1991;181:396-401. doi: 10.1016/s0006-291x(05)81432-9
1016 95. Pollack A, Kontorovich AR, Fuster V, Dec GW. Viral myocarditis--diagnosis, treatment
1017 options, and current controversies. Nat Rev Cardiol. 2015;12:670-680. doi:
1018 10.1038/nrcardio.2015.108
1019 96. Martens CR, Accornero F. Viruses in the Heart: Direct and Indirect Routes to Myocarditis
1020 and Heart Failure. Viruses. 2021;13. doi: 10.3390/v13101924
1021 97. Kearney MT, Cotton JM, Richardson PJ, Shah AM. Viral myocarditis and dilated
1022 cardiomyopathy: mechanisms, manifestations, and management. Postgrad Med J.
1023 2001;77:4-10. doi: 10.1136/pmj.77.903.4
1024 98. Kuhl U, Pauschinger M, Noutsias M, Seeberg B, Bock T, Lassner D, Poller W, Kandolf
1025 R, Schultheiss HP. High prevalence of viral genomes and multiple viral infections in the
1026 myocardium of adults with "idiopathic" left ventricular dysfunction. Circulation.
1027 2005;111:887-893. doi: 10.1161/01.CIR.0000155616.07901.35
1028 99. Xu CY, Zhang WS, Zhang H, Cao Y, Zhou HY. The Role of Connexin-43 in the
1029 Inflammatory Process: A New Potential Therapy to Influence Keratitis. J Ophthalmol.
1030 2019;2019:9312827. doi: 10.1155/2019/9312827
1031 100. Zhong C, Chang H, Wu Y, Zhou L, Wang Y, Wang M, Wu P, Qi Z, Zou J. Up-regulated
1032 Cx43 phosphorylation at Ser368 prolongs QRS duration in myocarditis. J Cell Mol Med.
1033 2018;22:3537-3547. doi: 10.1111/jcmm.13631
1034 101. Spurgeon ME, Ornelles DA. The adenovirus E1B 55-kilodalton and E4 open reading
1035 frame 6 proteins limit phosphorylation of eIF2alpha during the late phase of infection. J
1036 Virol. 2009;83:9970-9982. doi: 10.1128/JVI.01113-09
1037 102. Yueh A, Schneider RJ. Selective translation initiation by ribosome jumping in
1038 adenovirus-infected and heat-shocked cells. Genes Dev. 1996;10:1557-1567. doi:
1039 10.1101/gad.10.12.1557
1040 103. Huke S, Venkataraman R, Faggioni M, Bennuri S, Hwang HS, Baudenbacher F,
1041 Knollmann BC. Focal energy deprivation underlies arrhythmia susceptibility in mice with
1042 calcium-sensitized myofilaments. Circulation research. 2013;112:1334-1344. doi:
1043 10.1161/CIRCRESAHA.113.301055
1044 104. Brugada J, Mont L, Boersma L, Kirchhof C, Allessie MA. Differential effects of heptanol,
1045 potassium, and tetrodotoxin on reentrant ventricular tachycardia around a fixed obstacle
1046 in anisotropic myocardium. Circulation. 1991;84:1307-1318. doi:
1047 10.1161/01.cir.84.3.1307
1048 105. Boersma L, Brugada J, Abdollah H, Kirchhof C, Allessie M. Effects of heptanol, class Ic,
1049 and class III drugs on reentrant ventricular tachycardia. Importance of the excitable gap
1050 for the inducibility of double-wave reentry. Circulation. 1994;90:1012-1022. doi:
1051 10.1161/01.cir.90.2.1012
1052 106. Toure A, Cabo C. Effect of cell geometry on conduction velocity in a subcellular model of
1053 myocardium. IEEE Trans Biomed Eng. 2010;57:2107-2114. doi:
1054 10.1109/TBME.2010.2050064
1055 107. Hubbard ML, Ying W, Henriquez CS. Effect of gap junction distribution on impulse
1056 propagation in a monolayer of myocytes: a model study. Europace. 2007;9 Suppl 6:vi20-
1057 28. doi: 10.1093/europace/eum203
1058 108. Danave IR, Tiffany-Castiglioni E, Zenger E, Barhoumi R, Burghardt RC, Collisson EW.
1059 Feline immunodeficiency virus decreases cell-cell communication and mitochondrial
1060 membrane potential. J Virol. 1994;68:6745-6750. doi: 10.1128/JVI.68.10.6745-
1061 6750.1994
1062 109. Faccini AM, Cairney M, Ashrafi GH, Finbow ME, Campo MS, Pitts JD. The bovine
1063 papillomavirus type 4 E8 protein binds to ductin and causes loss of gap junctional

1064 intercellular communication in primary fibroblasts. J Virol. 1996;70:9041-9045. doi:
1065 10.1128/JVI.70.12.9041-9045.1996
1066 110. Knabb MT, Danielsen CA, McShane-Kay K, Mbuy GK, Woodruff RI. Herpes simplex
1067 virus-type 2 infectivity and agents that block gap junctional intercellular communication.
1068 Virus Res. 2007;124:212-219. doi: 10.1016/j.virusres.2006.11.006
1069 111. Crow DS, Beyer EC, Paul DL, Kobe SS, Lau AF. Phosphorylation of connexin43 gap
1070 junction protein in uninfected and Rous sarcoma virus-transformed mammalian
1071 fibroblasts. Mol Cell Biol. 1990;10:1754-1763. doi: 10.1128/mcb.10.4.1754-1763.1990
1072 112. Sun P, Dong L, MacDonald AI, Akbari S, Edward M, Hodgins MB, Johnstone SR,
1073 Graham SV. HPV16 E6 Controls the Gap Junction Protein Cx43 in Cervical Tumour
1074 Cells. Viruses. 2015;7:5243-5256. doi: 10.3390/v7102871
1075 113. Gallego C, Jaracz-Ros A, Lagana M, Mercier-Nome F, Domenichini S, Fumagalli A,
1076 Roingeard P, Herfs M, Pidoux G, Bachelerie F, et al. Reprogramming of connexin
1077 landscape fosters fast gap junction intercellular communication in human papillomavirus-
1078 infected epithelia. Front Cell Infect Microbiol. 2023;13:1138232. doi:
1079 10.3389/fcimb.2023.1138232
1080 114. Chang LS, Shenk T. The adenovirus DNA-binding protein stimulates the rate of
1081 transcription directed by adenovirus and adeno-associated virus promoters. J Virol.
1082 1990;64:2103-2109. doi: 10.1128/JVI.64.5.2103-2109.1990
1083 115. Logan J, Shenk T. Adenovirus tripartite leader sequence enhances translation of
1084 mRNAs late after infection. Proceedings of the National Academy of Sciences of the
1085 United States of America. 1984;81:3655-3659. doi: 10.1073/pnas.81.12.3655
1086 116. Blazquez AB, Vazquez-Calvo A, Martin-Acebes MA, Saiz JC. Pharmacological Inhibition
1087 of Protein Kinase C Reduces West Nile Virus Replication. Viruses. 2018;10. doi:
1088 10.3390/v10020091
1089 117. Blazquez AB, Saiz JC. Potential for Protein Kinase Pharmacological Regulation in
1090 Flaviviridae Infections. International journal of molecular sciences. 2020;21. doi:
1091 10.3390/ijms21249524
1092 118. Nakano MY, Boucke K, Suomalainen M, Stidwill RP, Greber UF. The first step of
1093 adenovirus type 2 disassembly occurs at the cell surface, independently of endocytosis
1094 and escape to the cytosol. J Virol. 2000;74:7085-7095. doi: 10.1128/jvi.74.15.7085-
1095 7095.2000
1096 119. Yousuf MA, Lee JS, Zhou X, Ramke M, Lee JY, Chodosh J, Rajaiya J. Protein Kinase C
1097 Signaling in Adenoviral Infection. Biochemistry. 2016;55:5938-5946. doi:
1098 10.1021/acs.biochem.6b00858
1099 120. Castagna M, Takai Y, Kaibuchi K, Sano K, Kikkawa U, Nishizuka Y. Direct activation of
1100 calcium-activated, phospholipid-dependent protein kinase by tumor-promoting phorbol
1101 esters. The Journal of biological chemistry. 1982;257:7847-7851.
1102 121. Black AR, Black JD. Protein kinase C signaling and cell cycle regulation. Front Immunol.
1103 2012;3:423. doi: 10.3389/fimmu.2012.00423
1104 122. Soh JW, Weinstein IB. Roles of specific isoforms of protein kinase C in the
1105 transcriptional control of cyclin D1 and related genes. The Journal of biological
1106 chemistry. 2003;278:34709-34716. doi: 10.1074/jbc.M302016200
1107 123. Grand RJ, Ibrahim AP, Taylor AM, Milner AE, Gregory CD, Gallimore PH, Turnell AS.
1108 Human cells arrest in S phase in response to adenovirus 12 E1A. Virology.
1109 1998;244:330-342. doi: 10.1006/viro.1998.9102
1110 124. Ben-Israel H, Kleinberger T. Adenovirus and cell cycle control. Front Biosci.
1111 2002;7:d1369-1395. doi: 10.2741/ben
1112 125. Zheng X, Rao XM, Gomez-Gutierrez JG, Hao H, McMasters KM, Zhou HS. Adenovirus
1113 E1B55K region is required to enhance cyclin E expression for efficient viral DNA
1114 replication. J Virol. 2008;82:3415-3427. doi: 10.1128/JVI.01708-07

1115 126. Pasumarthi KB, Field LJ. Cardiomyocyte cell cycle regulation. Circulation research.
1116 2002;90:1044-1054. doi: 10.1161/01.res.0000020201.44772.67
1117 127. Kaab S, Nuss HB, Chiamvimonvat N, O'Rourke B, Pak PH, Kass DA, Marban E,
1118 Tomaselli GF. Ionic mechanism of action potential prolongation in ventricular myocytes
1119 from dogs with pacing-induced heart failure. Circulation research. 1996;78:262-273. doi:
1120 10.1161/01.res.78.2.262
1121 128. Plaster NM, Tawil R, Tristani-Firouzi M, Canun S, Bendahhou S, Tsunoda A, Donaldson
1122 MR, Iannaccone ST, Brunt E, Barohn R, et al. Mutations in Kir2.1 cause the
1123 developmental and episodic electrical phenotypes of Andersen's syndrome. Cell.
1124 2001;105:511-519. doi: 10.1016/s0092-8674(01)00342-7
1125 129. Tristani-Firouzi M, Jensen JL, Donaldson MR, Sansone V, Meola G, Hahn A,
1126 Bendahhou S, Kwiecinski H, Fidzianska A, Plaster N, et al. Functional and clinical
1127 characterization of KCNJ2 mutations associated with LQT7 (Andersen syndrome). The
1128 Journal of clinical investigation. 2002;110:381-388. doi: 10.1172/JCI15183
1129 130. Tsuboi M, Antzelevitch C. Cellular basis for electrocardiographic and arrhythmic
1130 manifestations of Andersen-Tawil syndrome (LQT7). Heart Rhythm. 2006;3:328-335.
1131 doi: 10.1016/j.hrthm.2005.11.026
1132 131. Reilly L, Alvarado FJ, Lang D, Abozeid S, Van Ert H, Spellman C, Warden J, Makielski
1133 JC, Glukhov AV, Eckhardt LL. Genetic Loss of IK1 Causes Adrenergic-Induced Phase 3
1134 Early Afterdepolariz ations and Polymorphic and Bidirectional Ventricular Tachycardia.
1135 Circ Arrhythm Electrophysiol. 2020;13:e008638. doi: 10.1161/CIRCEP.120.008638
1136 132. Sanguinetti MC, Curran ME, Zou A, Shen J, Spector PS, Atkinson DL, Keating MT.
1137 Coassembly of K(V)LQT1 and minK (IsK) proteins to form cardiac I(Ks) potassium
1138 channel. Nature. 1996;384:80-83. doi: 10.1038/384080a0
1139 133. Sanguinetti MC. Dysfunction of delayed rectifier potassium channels in an inherited
1140 cardiac arrhythmia. Annals of the New York Academy of Sciences. 1999;868:406-413.
1141 doi: 10.1111/j.1749-6632.1999.tb11302.x
1142 134. Aromolaran AS, Subramanyam P, Chang DD, Kobertz WR, Colecraft HM. LQT1
1143 mutations in KCNQ1 C-terminus assembly domain suppress IKs using different
1144 mechanisms. Cardiovascular research. 2014;104:501-511. doi: 10.1093/cvr/cvu231
1145 135. Eleftherianos I, Won S, Chtarbanova S, Squiban B, Ocorr K, Bodmer R, Beutler B,
1146 Hoffmann JA, Imler JL. ATP-sensitive potassium channel (K(ATP))-dependent regulation
1147 of cardiotropic viral infections. Proceedings of the National Academy of Sciences of the
1148 United States of America. 2011;108:12024-12029. doi: 10.1073/pnas.1108926108
1149 136. Croker B, Crozat K, Berger M, Xia Y, Sovath S, Schaffer L, Eleftherianos I, Imler JL,
1150 Beutler B. ATP-sensitive potassium channels mediate survival during infection in
1151 mammals and insects. Nat Genet. 2007;39:1453-1460. doi: 10.1038/ng.2007.25
1152 137. Iwata M, Komori S, Unno T, Minamoto N, Ohashi H. Modification of membrane currents
1153 in mouse neuroblastoma cells following infection with rabies virus. Br J Pharmacol.
1154 1999;126:1691-1698. doi: 10.1038/sj.bjp.0702473
1155 138. Cahalan MD, Chandy KG. The functional network of ion channels in T lymphocytes.
1156 Immunol Rev. 2009;231:59-87. doi: 10.1111/j.1600-065X.2009.00816.x
1157 139. Cotton CU. Basolateral potassium channels and epithelial ion transport. Am J Respir
1158 Cell Mol Biol. 2000;23:270-272. doi: 10.1165/ajrcmb.23.3.f198
1159 140. Villalonga N, David M, Bielanska J, Vicente R, Comes N, Valenzuela C, Felipe A.
1160 Immunomodulation of voltage-dependent K+ channels in macrophages: molecular and
1161 biophysical consequences. J Gen Physiol. 2010;135:135-147. doi:
1162 10.1085/jgp.200910334
1163 141. Surawicz B. Role of potassium channels in cycle length dependent regulation of action
1164 potential duration in mammalian cardiac Purkinje and ventricular muscle fibres.
1165 Cardiovascular research. 1992;26:1021-1029. doi: 10.1093/cvr/26.11.1021

1166 142. Solan JL, Marquez-Rosado L, Sorgen PL, Thornton PJ, Gafken PR, Lampe PD.
1167 Phosphorylation at S365 is a gatekeeper event that changes the structure of Cx43 and
1168 prevents down-regulation by PKC. The Journal of cell biology. 2007;179:1301-1309. doi:
1169 10.1083/jcb.200707060
1170 143. Karle CA, Zitron E, Zhang W, Wendt-Nordahl G, Kathofer S, Thomas D, Gut B, Scholz
1171 E, Vahl CF, Katus HA, et al. Human cardiac inwardly-rectifying K+ channel Kir(2.1b) is
1172 inhibited by direct protein kinase C-dependent regulation in human isolated
1173 cardiomyocytes and in an expression system. Circulation. 2002;106:1493-1499. doi:
1174 10.1161/01.cir.0000029747.53262.5c
1175 144. Alvi F, Idkowiak-Baldys J, Baldys A, Raymond JR, Hannun YA. Regulation of membrane
1176 trafficking and endocytosis by protein kinase C: emerging role of the pericentrion, a
1177 novel protein kinase C-dependent subset of recycling endosomes. Cell Mol Life Sci.
1178 2007;64:263-270. doi: 10.1007/s00018-006-6363-5
1179 145. Mondal A, Dawson AR, Potts GK, Freiberger EC, Baker SF, Moser LA, Bernard KA,
1180 Coon JJ, Mehle A. Influenza virus recruits host protein kinase C to control assembly and
1181 activity of its replication machinery. Elife. 2017;6. doi: 10.7554/eLife.26910
1182 146. Sieczkarski SB, Brown HA, Whittaker GR. Role of protein kinase C betaII in influenza
1183 virus entry via late endosomes. J Virol. 2003;77:460-469. doi: 10.1128/jvi.77.1.460-
1184 469.2003
1185 147. San-Juan-Vergara H, Peeples ME, Lockey RF, Mohapatra SS. Protein kinase C-alpha
1186 activity is required for respiratory syncytial virus fusion to human bronchial epithelial
1187 cells. J Virol. 2004;78:13717-13726. doi: 10.1128/JVI.78.24.13717-13726.2004
1188 148. Bergelson JM, Cunningham JA, Droguett G, Kurt-Jones EA, Krithivas A, Hong JS,
1189 Horwitz MS, Crowell RL, Finberg RW. Isolation of a common receptor for Coxsackie B
1190 viruses and adenoviruses 2 and 5. Science. 1997;275:1320-1323.
1191 149. Tomko RP, Xu R, Philipson L. HCAR and MCAR: the human and mouse cellular
1192 receptors for subgroup C adenoviruses and group B coxsackieviruses. Proceedings of
1193 the National Academy of Sciences of the United States of America. 1997;94:3352-3356.
1194 doi: 10.1073/pnas.94.7.3352
1195 150. Lyle C, McCormick F. Integrin alphavbeta5 is a primary receptor for adenovirus in CAR-
1196 negative cells. Virol J. 2010;7:148. doi: 10.1186/1743-422X-7-148
1197 151. Lim BK, Xiong D, Dorner A, Youn TJ, Yung A, Liu TI, Gu Y, Dalton ND, Wright AT,
1198 Evans SM, et al. Coxsackievirus and adenovirus receptor (CAR) mediates
1199 atrioventricular-node function and connexin 45 localization in the murine heart. The
1200 Journal of clinical investigation. 2008;118:2758-2770. doi: 10.1172/JCI34777
1201 152. Dorner AA, Wegmann F, Butz S, Wolburg-Buchholz K, Wolburg H, Mack A, Nasdala I,
1202 August B, Westermann J, Rathjen FG, et al. Coxsackievirus-adenovirus receptor (CAR)
1203 is essential for early embryonic cardiac development. Journal of cell science.
1204 2005;118:3509-3521. doi: 10.1242/jcs.02476
1205 153. Lisewski U, Shi Y, Wrackmeyer U, Fischer R, Chen C, Schirdewan A, Juttner R, Rathjen
1206 F, Poller W, Radke MH, et al. The tight junction protein CAR regulates cardiac
1207 conduction and cell-cell communication. J Exp Med. 2008;205:2369-2379. doi:
1208 10.1084/jem.20080897
1209 154. Ortiz-Zapater E, Santis G, Parsons M. CAR: A key regulator of adhesion and
1210 inflammation. Int J Biochem Cell Biol. 2017;89:1-5. doi: 10.1016/j.biocel.2017.05.025
1211 155. Guglielmi KM, Johnson EM, Stehle T, Dermody TS. Attachment and cell entry of
1212 mammalian orthoreovirus. Curr Top Microbiol Immunol. 2006;309:1-38. doi: 10.1007/3-
1213 540-30773-7_1
1214 156. Baty CJ, Sherry B. Cytopathogenic effect in cardiac myocytes but not in cardiac
1215 fibroblasts is correlated with reovirus-induced acute myocarditis. J Virol. 1993;67:6295-
1216 6298. doi: 10.1128/JVI.67.10.6295-6298.1993

1217 157. Sherry B, Baty CJ, Blum MA. Reovirus-induced acute myocarditis in mice correlates with
1218 viral RNA synthesis rather than generation of infectious virus in cardiac myocytes. J
1219 Virol. 1996;70:6709-6715. doi: 10.1128/JVI.70.10.6709-6715.1996
1220 158. McCarthy MK, Malitz DH, Molloy CT, Procario MC, Greiner KE, Zhang L, Wang P, Day
1221 SM, Powell SR, Weinberg JB. Interferon-dependent immunoproteasome activity during
1222 mouse adenovirus type 1 infection. Virology. 2016;498:57-68. doi:
1223 10.1016/j.virol.2016.08.009
1224 159. Hemmi S, Spindler KR. Murine adenoviruses: tools for studying adenovirus
1225 pathogenesis in a natural host. FEBS letters. 2019;593:3649-3659. doi: 10.1002/1873-
1226 3468.13699

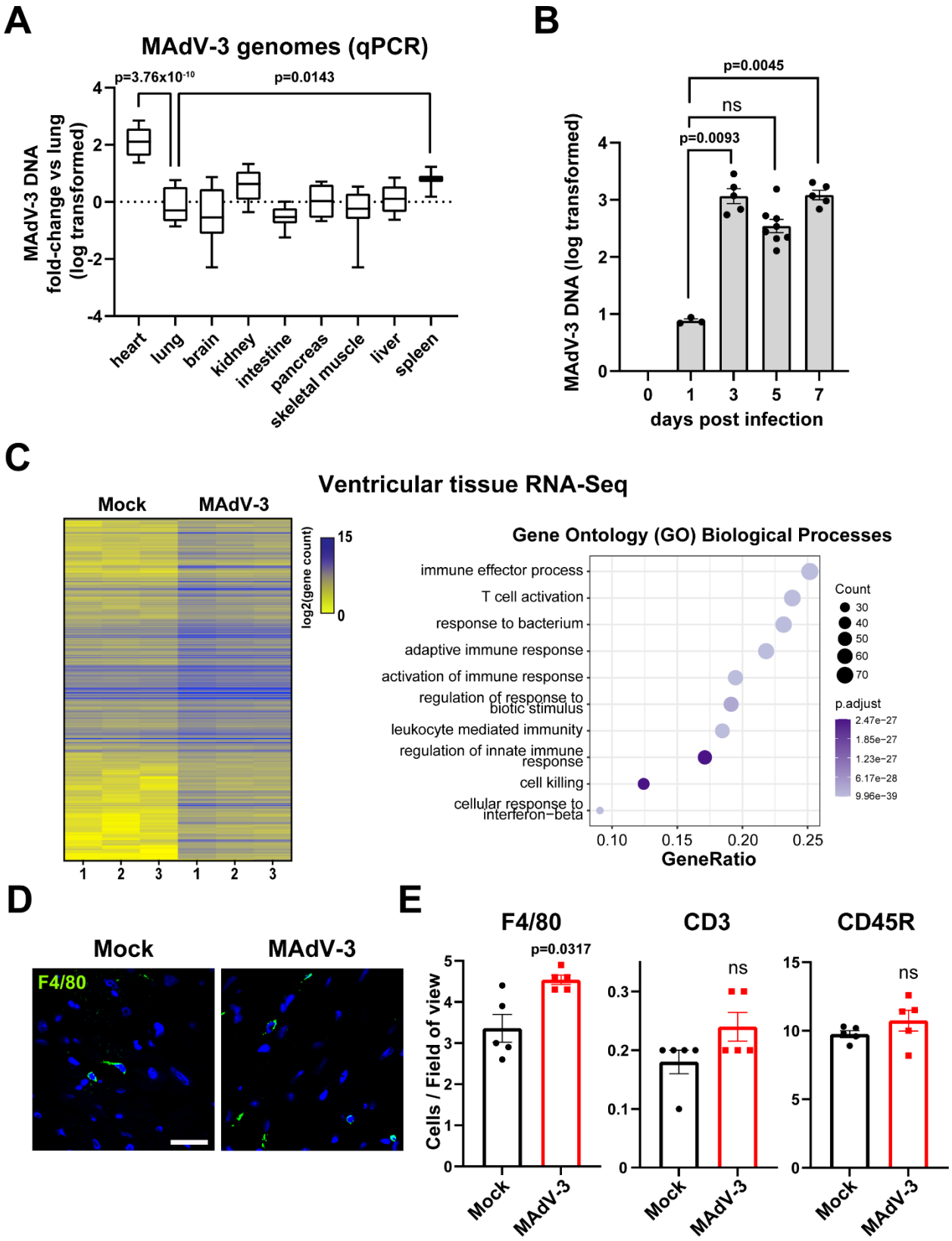
A
MAdV-3 genomes (qPCR)
p=3.76x10-10
p=0.0143
MAdV-3 DNA fold-change vs lung (log transformed)
4
2
0
-2
-4
heart
lung
brain
kidney
intestine
pancreas
skeletal muscle
liver
spleen
B
p=0.0045
ns
p=0.0093
MAdV-3 DNA (log transformed)
4
3
2
1
0
0
1
3
5
7
days post infection
C
Ventricular tissue RNA-Seq
Mock
MAdV-3
log2(gene count)
15
0
1
2
3
1
2
3
Gene Ontology (GO) Biological Processes
immune effector process
T cell activation
response to bacterium
adaptive immune response
activation of immune response
regulation of response to biotic stimulus
leukocyte mediated immunity
regulation of innate immune response
cell killing
cellular response to interferon-beta
0.10
0.15
0.20
0.25
GeneRatio
Count
30
40
50
60
70
p.adjust
2.47e-27
1.85e-27
1.23e-27
6.17e-28
9.96e-39
D
Mock
MAdV-3
F4/80
E
F4/80
CD3
CD45R
p=0.0317
ns
ns
Cells / Field of view
5
4
3
2
1
0
0.3
0.2
0.1
0
15
10
5
0
Mock
MAdV-3
Mock
MAdV-3
Mock
MAdV-3

Figure 1. Mouse adenovirus type-3 is cardiotropic and does not invoke an appreciable infiltrative cardiac immune response during acute infection. Mice were infected retro-orbitally with $5x10^5$ i.u. MAdV-3 or saline (mock) and tissues were harvested 7 d.p.i. **A)** Using quantitative PCR, MAdV-3 viral genomes were measured across major organs and compared to organ lung tissue as a reference. (heart n=10, lung n=8, brain n=10, kidney n=10, intestine n=10, pancreas n=4, skeletal muscle n=8, liver n=12, spleen n=10). **B)** In heart tissue alone, MAdV-3 viral genomes were quantified by qPCR over a 7 day time course. **C)** RNA-Seq from ventricular tissue from control and infected animals (n=3). Left: heat map of the log2-transformed gene counts for all significant differentially expressed genes (DEGs) in infected animals compared to control (adjusted p-value < 0.05, absolute log2 fold change > 1.0). Right: gene ontology (GO) plot demonstrating the top 10 significant GO terms for biological processes identified through over-representation analysis using significant DEGs. **D)** Confocal immunofluorescence microscopy of ventricular cryosections labeled for infiltrating macrophages (F4/80, green; scale bar: 25 μm). **E)** Quantification of numbers of F4/80+, CD3+, and CD45R+ cells per field of view from confocal immunofluorescence microscopy. (n=5; 10 fields of view per heart). (**A**), One-way ANOVA with Dunnett's multiple comparisons test ****$p = 3.76x10^{-10}$, * $p = 1.43x10^{-2}$ (**B**), Kruskal-Wallis with Dunnett's multiple comparisons test ** day 3 $p= 9.32x10^{-3}$, ** day 7 $p = 4.45x10^{-3}$ (**E**). Mann Whitney test F4/80+ *$p = 3.17x10^{-2}$. Data are represented as mean ± SEM.

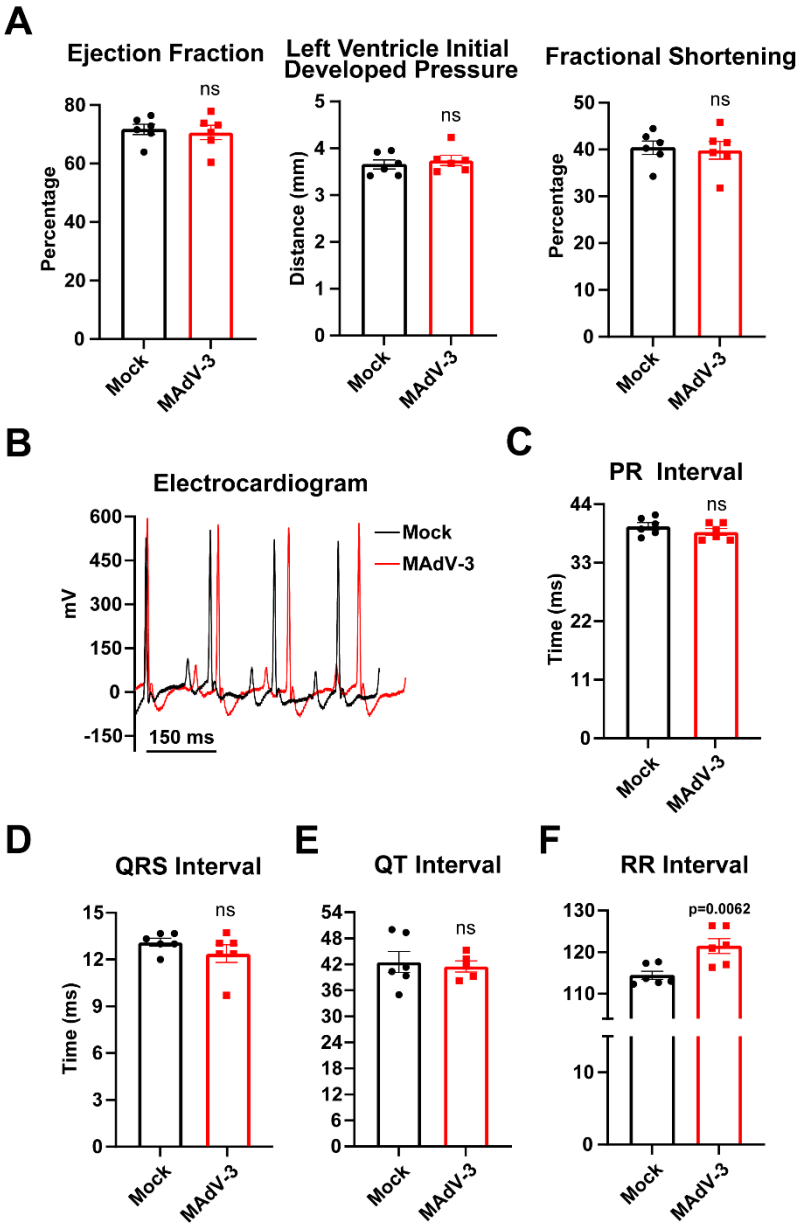

Figure 2. Acute cardiac adenoviral infection slows heart rate but does not alter ECG morphology or induce gross cardiomyopathy. *In vivo* echocardiography and electrocardiography were performed 7 d.p.i. in mock- or MAdV-3-infected mice. **A)** Cardiac function was measured by echocardiography on lightly anesthetized mock- and MAdV-3-infected mice (n=6). **B)** Representative *in vivo* electrocardiography measurements from lightly anesthetized mock- and MAdv-3-infected mice using paw pad electrodes. **C-F)** Quantification of PR, QRS, QT, and RR intervals from **B**. **p = 6.2×10^{-3}, student's t-test (n=6).

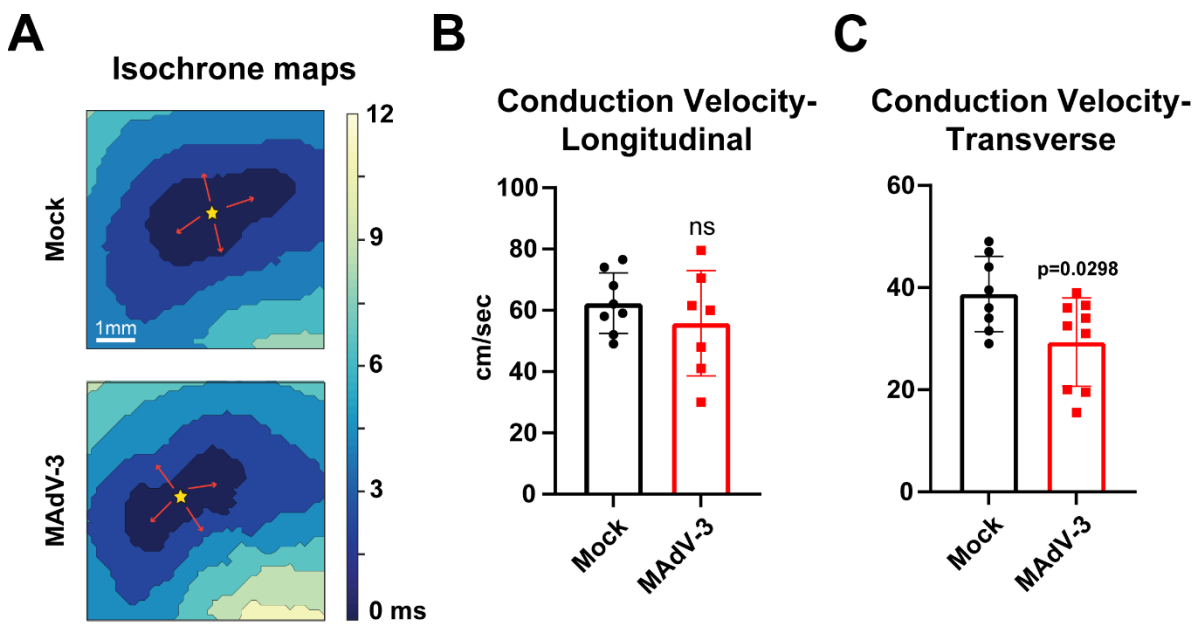

Figure 3. Acute cardiac adenoviral infection results in reduced ventricular conduction velocity. *Ex vivo* optical mapping was performed on Langendorff-perfused hearts 7 d.p.i. from mock- or MAdV-3-infected mice. **A)** Example isochrones maps paced at a cycle length of 150 ms with 1 ms pulse duration. **B, C)** Conduction velocity in longitudinal (CVL)and transverse (CVT) directions was quantified (n=8,9). * $p = 2.98 \times 10^{-2}$, student's t-test. Data are represented as mean ± SEM.

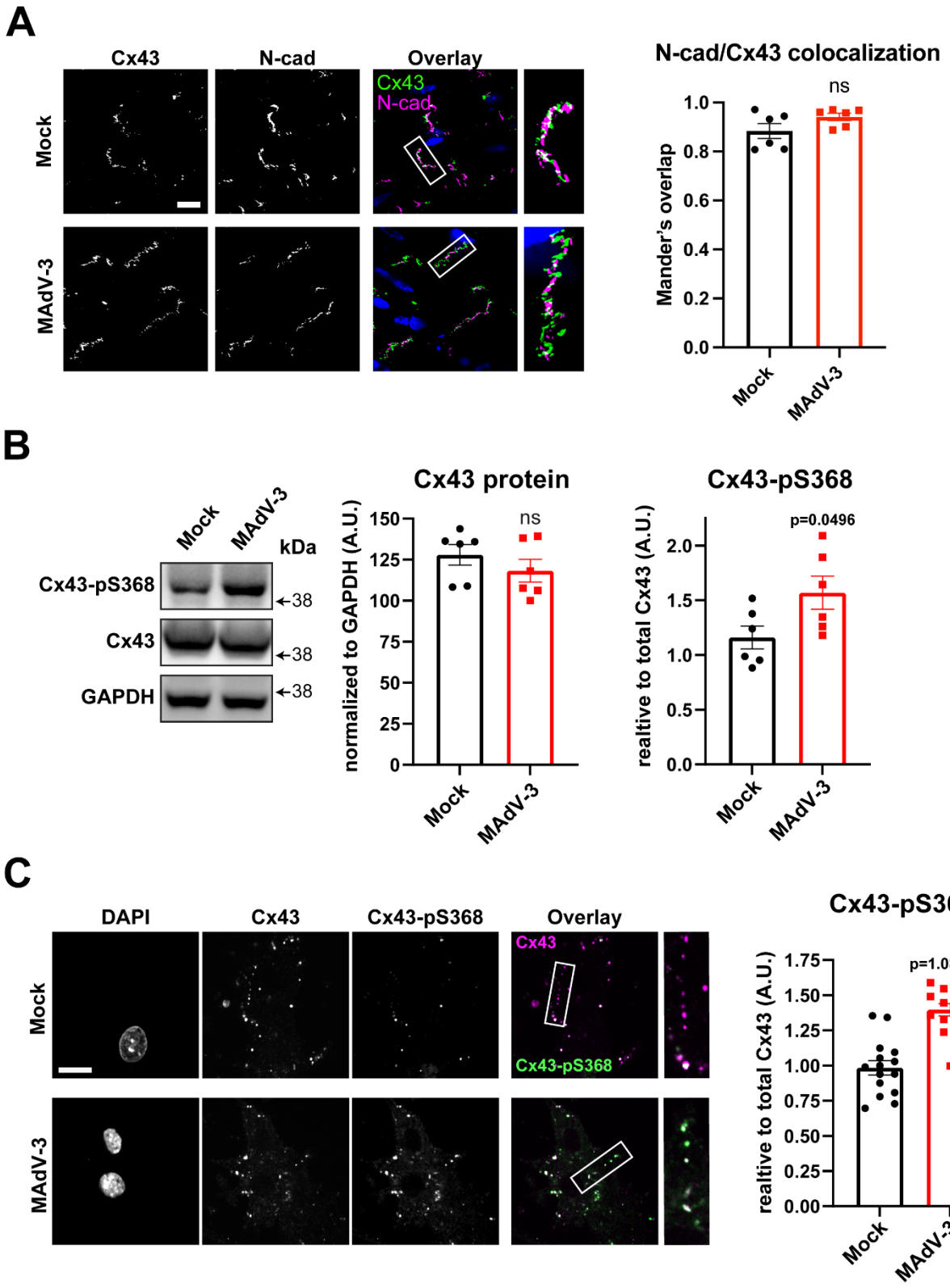
A
Cx43
N-cad
Overlay
Mock
MAdV-3
Cx43
N-cad
N-cad/Cx43 colocalization
ns
Mander's overlap
1.0
0.8
0.6
0.4
0.2
0.0
Mock
MAdV-3
B
Mock
MAdV-3
kDa
Cx43-pS368
Cx43
GAPDH
←38
Cx43 protein
ns
normalized to GAPDH (A.U.)
150
125
100
75
50
25
0
Cx43-pS368
p=0.0496
realtive to total Cx43 (A.U.)
2.0
1.5
1.0
0.5
0.0
C
DAPI
Cx43
Cx43-pS368
Overlay
Cx43
Cx43-pS368
Cx43-pS368
p=1.08x10-6
realtive to total Cx43 (A.U.)
1.75
1.50
1.25
1.00
0.75
0.50
0.25
0.00

Figure 4. Acute adenovirus infection elicits increased connexin43 Ser368 phosphorylation in hearts and primary cardiomyocytes. Mice were infected retro-orbitally with $5x10^5$ i.u. MAdV-3 or saline (mock) and cardiac tissue was harvested 7 d.p.i. for analyses. **A)** SORA confocal microscopy of Cx43 (green) and N-cadherin (magenta) with quantification of colocalization by Mander's coefficient (scale bar 10 µm; n=6), not significant Mann-Whitney test. **B)** Western blotting of cardiac ventricle tissue probed for phospho-Cx43 Ser368, Cx43, with GAPDH as loading control to normalize total Cx43 quantitation on left and phospho-Cx43 Ser368 normalized to total on right (n=6). student's t-test. $*p = 4.96x10^{-2}$, **C)** Confocal immunofluorescence microscopy of primary mouse neonatal ventricular cardiomyocytes 24 h.p.i. with MAdV-3 labeled for total Cx43 (magenta) and phospho-Cx43 Ser368 (green) (scale bar: 25 µm; n=3; **** $1.08x10^{-6}$ **B,C)** Data are represented as mean ± SEM.

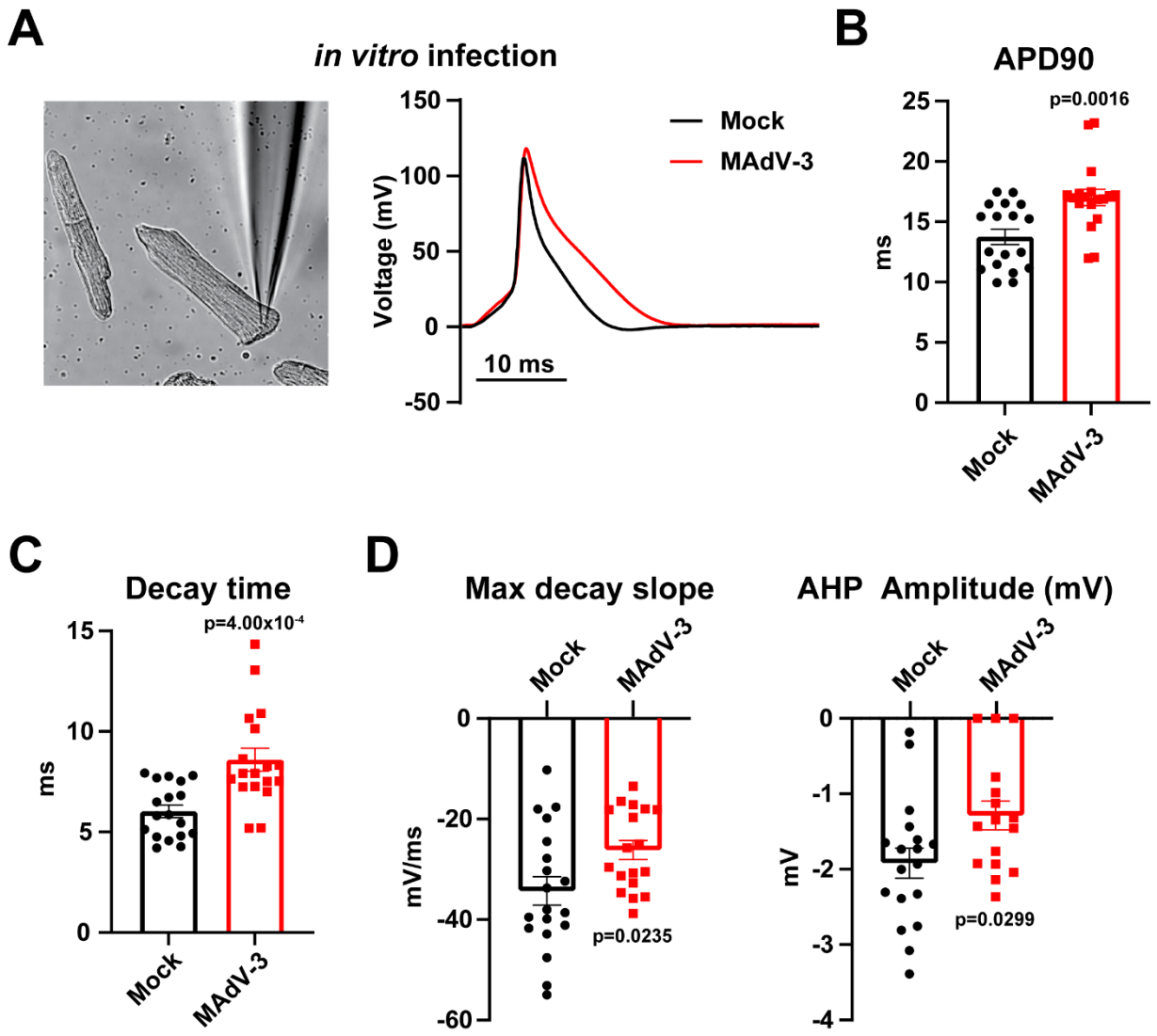

Figure 5. Acute mouse adenovirus infection alters ion channel gene expression *in vivo and* prolongs ventricular cardiomyocyte action potential duration *in vitro*. Isolated ACMs were either infected with MAdV-3 at an MOI 10 or not and harvested 24 h.p.i. *in vitro*. **A)** Representative image of ACMs used for patch clamp experiments with representative action potential traces recorded from uninfected (black) and MAdV-3-infected (red) cells. **B)** Action potential duration at 90% repolarization was recorded in uninfected and MAdV-3-infected ACMs (n=18). Mann-Whitney U test **$p = 1.60 \times 10^{-3}$ **C)** Decay time was recorded in uninfected and MAdV-3-infected ACMs (n=18). *** $p = 4.00 \times 10^{-4}$ **D)** Max decay slope and afterpolarization amplitude was recorded in uninfected and MAdV-3-infected ACMs (n=18). Max decay slope * $p = 2.35 \times 10^{-2}$, AHP amplitude * $p = 2.99 \times 10^{-2}$ student's t-test. Data are represented as mean ± SEM.

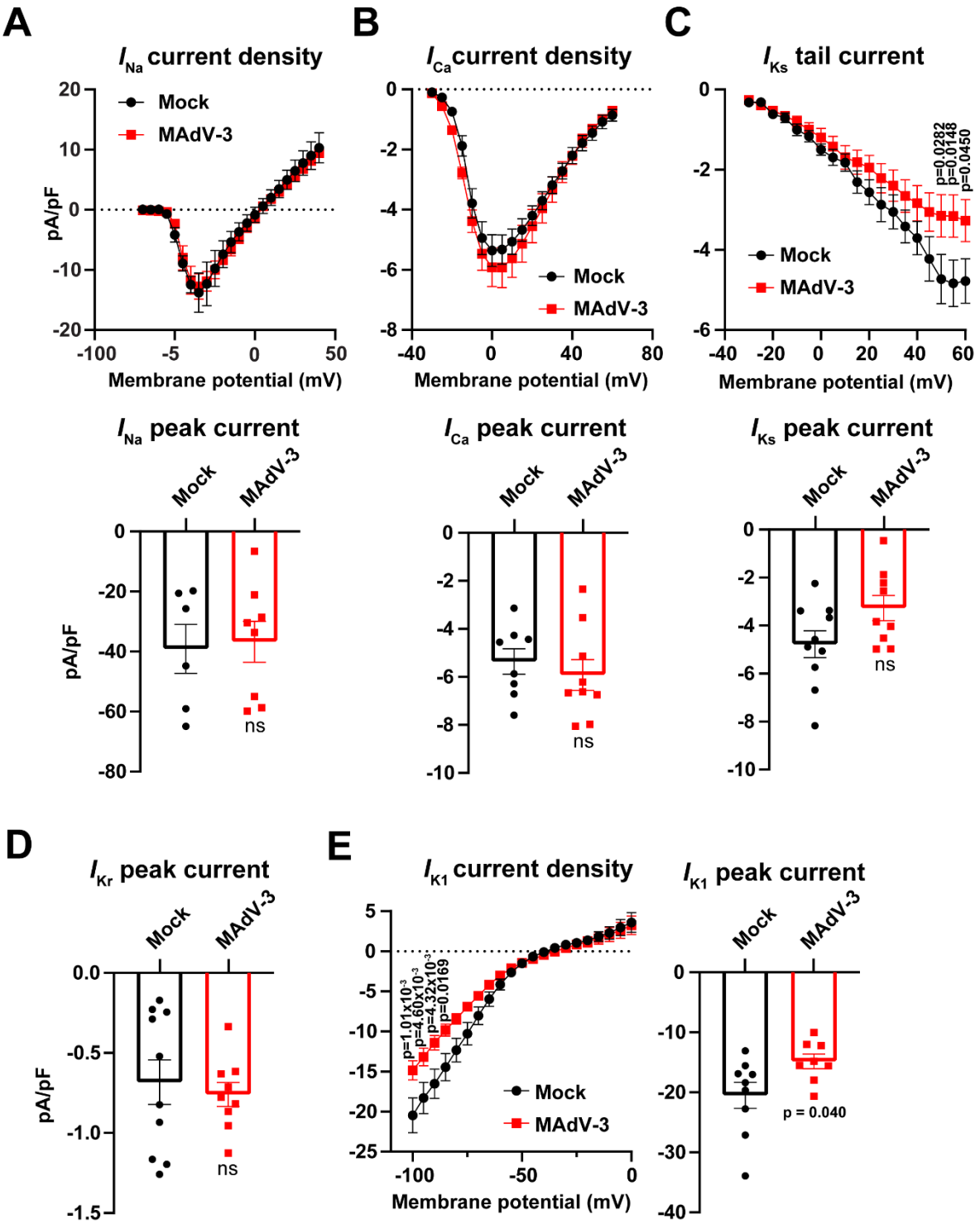
A
I_{Na} current density
Mock
MAdV-3
pA/pF
Membrane potential (mV)
B
I_{Ca} current density
Mock
MAdV-3
Membrane potential (mV)
C
I_{Ks} tail current
p=0.0282
p=0.0148
p=0.0450
Mock
MAdV-3
Membrane potential (mV)
I_{Na} peak current
Mock
MAdV-3
pA/pF
ns
I_{Ca} peak current
Mock
MAdV-3
ns
I_{Ks} peak current
Mock
MAdV-3
ns
D
I_{Kr} peak current
Mock
MAdV-3
pA/pF
ns
E
I_{K1} current density
p=1.01x10-3
p=4.60x10-3
p=4.32x10-3
p=0.0169
Mock
MAdV-3
Membrane potential (mV)
I_{K1} peak current
Mock
MAdV-3
p = 0.040

Figure 6. Acute mouse adenovirus infection decreases I_{K1} and I_{KS} current density in isolated adult mouse cardiomyocytes. Isolated ACMs were infected with MAdV-3 at an MOI 10 and analyzed 24 h.p.i. **A)** Current density measured isolated ACMs at 24 h.p.i. for I_{Na}, n=6,8. **B)** Current density measured isolated ACMs at 24 h.p.i. for I_{Ca}, n=8,9 **C)** Current density measured isolated ACMs at 24 h.p.i. for I_{Ks},n=10, 9, Two-way ANOVA with Šídák's multiple comparisons test adjusted *p value= $2.82x10^{-2}$, $1.48x10^{-2}$, $4.50x10^{-2}$, D) Current density measured isolated ACMs at 24 h.p.i. for I_{Kr}, n=10,9 **E**) Current density measured isolated ACMs at 24 h.p.i. for I_{K1}, n=9,8. , Two-way ANOVA with Šídák's multiple comparisons test adjusted * p value = $1.01x10^{-3}$, $4.60x10^{-3}$, $4.32x10^{-3}$, $1.69x10^{-2}$ Peak current I_{K1} student's t-test * p = $4.00x10^{-2}$. Data are represented as mean ±SEM.

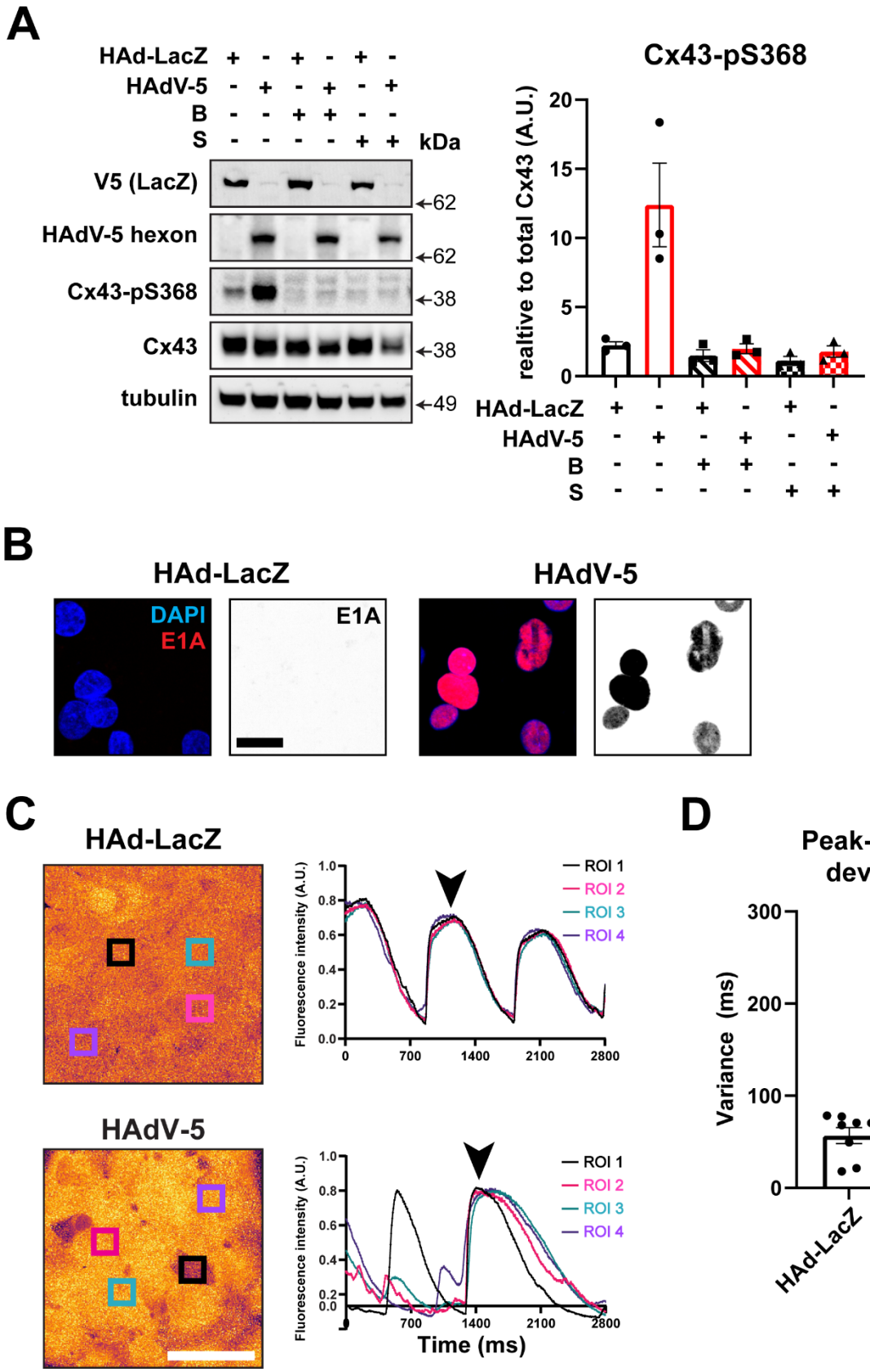
A
HAd-LacZ + - + - + -
HAdV-5 - + - + - +
B - - + + - -
S - - - - + +
kDa
V5 (LacZ)
HAdV-5 hexon
Cx43-pS368
Cx43
tubulin
62
62
38
38
49
Cx43-pS368
realtive to total Cx43 (A.U.)
20
15
10
5
0
HAd-LacZ + - + - + -
HAdV-5 - + - + - +
B - - + + - -
S - - - - + +
B
HAd-LacZ
HAdV-5
DAPI
E1A
E1A
C
HAd-LacZ
HAdV-5
Fluorescence intensity (A.U.)
1.0
0.8
0.6
0.4
0.2
0.0
0
700
1400
2100
2800
ROI 1
ROI 2
ROI 3
ROI 4
Time (ms)
D
Peak-to-peak deviation
Variance (ms)
300
200
100
0
p = 3.11x10-4
HAd-LacZ
HAdV-5

Figure 7. Human Adenovirus Type-5 infection increases Cx43-Ser368 phosphorylation through PKC activation and uncouples HiPSC-derived cardiomyocytes.
HiPSC-CMs were infected with HAdV-LacZ or HAdV-5 at an MOI 10 and studies performed 24 h.p.i. **A)** PKC inhibitors bisindolylmaleimide VIII “B” or sotrastaurin “S” were added 1 h post infection. Western blotting of cells probed for phospho-Cx43 Ser368 with quantification normalized to total Cx43 on right (n=3), Kruskal-Wallis with Dunnett's multiple comparisons test. **B)** Confocal immunofluorescence microscopy from fixed HiPSC-CMs to detect nuclei (blue) and Human Adenoviral protein E1A (red) (scale bar: 25 µm). **C)** Live-cell confocal microscopy 24 h.p.i. using Fluo-4 AM to measure Ca^{2+} transients and quantification of fluorescence signaling over time in one field of view. Black arrowheads indicate peak fluorescence timepoints where representative images are taken from (scale bar: 80 µm). **D)** Average peak-to-peak fluorescence intensity variance measured per cell over time (n=8,9). Mann Whitney test *** $p = 3.11 \times 10^{-4}$ (**D**). Data are represented as mean ± SEM.

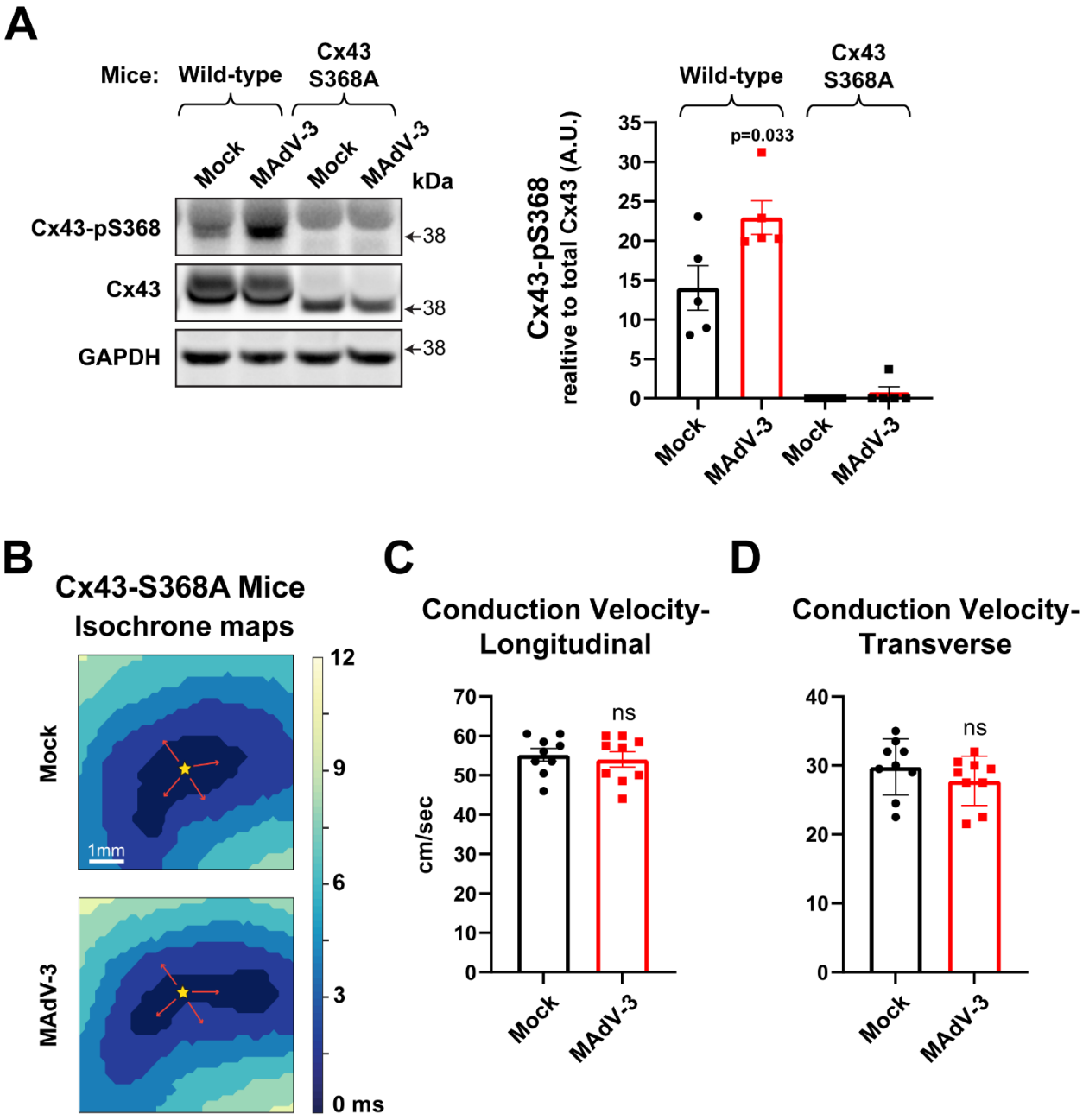
A
Mice:
Wild-type
Cx43 S368A
Mock
MAdV-3
Mock
MAdV-3
kDa
Cx43-pS368
Cx43
GAPDH
38
38
38
Wild-type
Cx43 S368A
Cx43-pS368
realtive to total Cx43 (A.U.)
p=0.033
35
30
25
20
15
10
5
0
Mock
MAdV-3
Mock
MAdV-3
B
Cx43-S368A Mice
Isochrone maps
Mock
MAdV-3
1mm
12
9
6
3
0 ms
C
Conduction Velocity-Longitudinal
cm/sec
70
60
50
40
30
20
10
0
ns
Mock
MAdV-3
D
Conduction Velocity-Transverse
40
30
20
10
0
ns
Mock
MAdV-3

Figure 8. Ablation of Cx43 Ser368 phosphorylation protects against cardiac conduction slowing during acute MAdV-3 infection. Western blotting and e*x vivo* optical mapping was performed hearts 7 d.p.i. from mock- or MAdV-3-infected wild-type mice and mice harboring a Cx43-Ser368-Ala mutation. **A)** of cardiac ventricle tissue probed for phospho-Cx43 Ser368, total Cx43, and GAPDH as loading control with quantification of phospho-Cx43 Ser368 normalized to total Cx43 on right (n=5). **B)** Example isochrones maps paced at a cycle length of 150 ms with 1 ms pulse duration. **C, D)** Conduction velocity in longitudinal (CVL)and transverse (CVT) directions was quantified (n=9,9). * $p = 3.30x10^{-2}$, (**A**), student's t-test (**C**, **D**). Data are represented as mean ± SEM.

Supplemental Materials

Acute adenoviral infection elicits an arrhythmogenic substrate prior to myocarditis.

Rachel L. Padget, Michael J. Zeitz, Grace A. Blair, Xiaobo Wu, Michael D. North, Mira T. Tanenbaum, Kari E. Stanley, Chelsea M. Phillips, D. Ryan King, Samy Lamouille, Robert G. Gourdie, Gregory S. Hoeker, Sharon A. Swanger, Steven Poelzing, James W. Smyth

Expanded Materials and Methods

Animals

All animal husbandry and experimental protocols described utilized 8-12 week old C57BL/6J male and female mice (initially obtained from The Jackson Laboratory and subsequently bred in house), were carried out under NIH guidelines, and approved by the Virginia Tech Institutional Animal Care and Use Committee. Cx43-S368A (also termed 'PKC' mice in prior literature) mice were a generous gift from Dr. Paul Lampe, Fred Hutchinson Cancer Center, Seattle, WA[62].

Cell culture

Normal murine mammary gland (NMuMG), A549, (ATCC), 3T6, 293A, and 293FT (Thermo Fisher) were maintained in Dulbecco's Modified Eagle Medium, high glucose with L-glutamine and sodium pyruvate (Genesee Scientific) supplemented with 10% FBS, non-essential amino acids (Gibco) and Mycozap Plus-CL (Lonza). Primary mouse neonatal ventricular cardiomyocytes were isolated as previously described[63] and maintained in F12/DMEM 50/50 supplemented with 2 % FBS (Gibco), insulin–transferrin–sodium selenite media supplement, 10 μM BrdU, 20 μM cytosine β-darabinofuranoside (Sigma-Aldrich), and Mycozap-PR (Lonza). BrdU and cytosine β-darabinofuranoside were removed 24 h prior to MAdV-3 infection studies.

HiPSC-CM differentiation, expansion, and maturation

HiPSCs (Cell Applications) were differentiated into cardiomyocytes as previously described[64], with modifications. Briefly, iPSCs were seeded in E8 medium (Thermo Fisher) into matrigel (Corning) coated (1:99) 12-well plates with daily media changes for 3 days. Following this, on day 0, medium was changed to CDM3, as defined in[65] with 3 μM CHIR-99021 (Selleckchem) in RPMI for 2 days. On day 2, medium was changed to CDM3 with 2 μM Wnt-C59 (Cayman). On day 4, medium was replaced with CDM3. On day 6, medium was changed to RPMI1640 + B27 (Thermo Fisher) (- insulin) and refreshed on day 8. On day 10, medium was changed to RPMI1640 without glucose + B27. On day 12, cardiomyocytes were expanded as in[66]. Cells were lifted with TrypLE Select Enzyme 10X (Thermo Fisher), washed with PBS 20% FBS and centrifuged at 200 x *g* for 4 min, resuspended in RPMI 1640 + B27 1X with 10% Knock Out Serum Replacement (Gibco) and Thiazovivin 1.0 μM (Selleckchem), and transferred into 10 cm dishes. 24 h later medium was replaced with RPMI 1640 + B27 1X supplemented with 2 μM CHIR-99021 (Selleckchem). Cells were further expanded for 4 passages prior to cryopreservation. IPSC-CMs were verified by the presence of cardiac troponin-T, N-cadherin, and spontaneous contraction under phase microscopy. Prior to experiments, IPSC-CMs were matured in a defined maturation medium composed of oxidative substrates and low glucose for 3 weeks with media changes every 3 days, as previously reported[67].

Virus propagation and titering

MAdV-3 (a generous gift from D. H. Krüger, M.D., Ph.D., Institute of Med. Virology, University Hospital Charité, Berlin) was propagated in NMuMG cells. MAdV-3 was purified by PEGylation and CsCl ultracentrifugation as previously described, and titer was determined by immunofluorescence confocal microscopy in 3T6 cells (Thermo Fisher)[38,68]. HAd5 (ATCC) was propagated in A549 cells and AdlacZ was generated according to manufacturer's instructions from pAd/CMV/V5-GW/LacZ (Thermo Fisher) for purification by CsCl ultracentrifugation and titering in 293A cells as previously described[38,68].

Adult mouse cardiomyocyte isolations

Adult mouse cardiomyocytes (ACMs) were isolated as previously described[69]. In brief, mice were anesthetized with isoflurane and administered a 500 U heparin i.p. injection (Sigma Aldrich). Hearts were excised and cannulated within 4 min post excision on a Langendorff

apparatus utilizing pH 7.4 perfusion buffer for 3 min comprising (in mM, all from Sigma Aldrich): NaCl (120.4), KCl (12.7), KH_2PO_4 (0.6), Na_2HPO_4 (0.6), $MgSO_4$-$7H_2O$ (1.2), $NaHCO_3$ (4.6), Taurine (30), Glucose (5.5), 2,3-Butanedione 2-monoxime (BDM, 10), and HEPES (10). Perfusate was then switched to perfusion buffer including 2.4 mg/ml Type II Collagenase (Worthington Biochemical) followed with 3 μM $CaCl_2$ reintroduction when 20 mL of solution remain to perfuse. Aorta, vena cava, and atria were removed, and the ventricles were mechanical broken apart into single cells. Cells were centrifuged at 30 x *g* for 3 min, and resuspended in three sequential stop buffers comprised of perfusion buffer and FBS + 10, 40, 100 μM $CaCl_2$ reintroduction steps were completed and cells were plated on dishes coated with 100 μg/ml laminin (Gibco) in cardiac myocyte media (CMM, ScienCell) with provided cardiac myocyte growth supplement, 5% FBS, 50 mM BDM, and MyocoZap Plus-PR (Lonza), which was replaced on cardiac myocytes at 2 h after plating.

Infections and inhibitor treatments

In vivo

8-12 week old C57BL/6 male and female mice were anesthetized and inoculated via retro-orbital injection with 5×10^5 infectious units (i.u.) of MAdV-3 diluted in 0.9 % sterile saline (Teknova) or saline solution alone for control animals, using U-100 Insulin syringes (BD). Mice were monitored daily for weight loss and assessment of fur ruffling/neurological symptoms, none of which were noted in the work described herein.

In vitro

Infections were performed at a multiplicity of infection (M.O.I.) of 10 i.u./cell as previously described[38]. For PKC-inhibition experiments IPSC-CMs were seeded in 12-well culture plates at 90 % confluency and matured. Cells were treated with 5 μM Bisindolylmaleimide VIII (E2839; Selleckchem) or 5 μM sotrastaurin (S2791; Selleckchem) 1 h post infection with Ad5 or LacZ. After 24 h protein was harvested, and western blotting performed as described below.

RNA-Seq

Ventricles were separated from atria and snap frozen for RNA-seq processing by GeneWiz, Inc. who performed alignment and initial analyses. Sequencing was performed by HiSeq 2x150 PE HO HiSeq 2x150 bp configuration. DESeq2 was used to compare gene expression between groups of samples. The Wald test was used to generate p-values and log2 fold changes. Genes with an adjusted p-value < 0.05 and absolute log2 fold change > 1 were called as differentially expressed. Log2 transformed normalized gene counts of significant differentially expressed genes were hierarchically clustered using the heatmap program clustergrammer[70], with the Scipy library in Python, using default settings of cosine distance and average linkage. Over-representation analysis was conducted with significant differentially expressed genes using the R/Bioconductor package clusterProfiler[71], with p-values adjusted using the Benjamini-Hochberg method. The top ten most significant gene ontology terms for biological processes were plotted in order of descending gene ratio.

Cytokine array

Mouse hearts were excised, rinsed in ice-cold PBS and snap frozen for downstream use in cytokine array. Ventricle tissue was lysed and array performed according to manufacturer's instructions (ab133993; Abcam) and developed and quantified utilizing a Chemidoc MP imaging system with Image Lab software (Bio-Rad).

Cardiac Troponin I and humoral immune response ELISAs

Mouse serum was processed from blood collected from the mandibular vein and heart excision of mock and MAdV-3 infected animals. Cardiac Troponin I (cTNI) serum levels were measured

using a sandwich ELISA according to manufacturer's instructions (ab246529, Abcam). The antiviral humoral response was detected as previously described with modifications utilizing the OptEIA Reagent Set B (BD Biosciences)[72]. Briefly, 96-well plates were coated with UV-inactivated purified MAdV-3 at 1 x 10^4 i.u./well overnight in 100 mM sodium carbonate coating buffer at 4 °C overnight an washed three times before blocking for 1 h in assay diluent. Serum samples were diluted 1/500 in assay diluent and 100 µl added to each well in triplicate, and incubated for 1 h at room temperature before 3 washes. Secondary antibody (HRP conjugated goat anti-mouse IgG, 1/3,000; Abcam) was diluted in assay diluent, 100 µl added to each well, and incubated for 1 at room temperature before 3 washes and substrate development according to manufacturer's instructions. Data for both ELISAs were acquired utilizing a SpectraMax i3 plate reader (Molecular Devices).

Echocardiography

Echocardiography was performed and analyzed using VisualSonics Vevo 660 High-Resolution Imaging System with a MS250 transducer at 7 days post-infection. Mice were anesthetized with 2 % isoflurane in 2 % supplemental O_2 with long axis and M-mode images recorded, and surface electrodes measured cardiac electrical activity as previously reported[73]. Heart rate, electrocardiography, and left ventricle (LV) dimensions of ejection fractions (EF %), fractional shortening (FS %), left ventricular developed pressure (LVDP) at diastole were measured.

Histology

Histological preparation, blood counts, and serum chemistry analysis were performed according to standard operating procedures in the Virginia Tech Animal Laboratory Services (ViTALs) diagnostic laboratory accredited by the American Association of Veterinary Laboratory Diagnosticians (AAVLD) at Virginia-Maryland College of Veterinary Medicine. Tissues for histology were fixed in 10 % neutral buffered formalin (VWR) for 24 h, then trimmed, processed, paraffin-embedded, and sectioned at 5 µm prior to staining with hematoxylin and eosin (Abcam). Histopathologic examination was performed in a blinded fashion by a board-certified veterinary pathologist. Tissues evaluated included heart, brain, lungs, thymus, salivary glands, esophagus, tongue, eyes, spleen, adipose tissue, liver, kidneys, adrenal glands, pancreas, stomach, duodenum, jejunum, ileum, colon, skeletal muscle, bone, bone marrow, and haired skin.

Tissue DNA extraction and qPCR for viral genomes

For viral tropism, tissue was homogenized in TRIzol (Thermo Fisher) and DNA was extracted according to manufacturer's instructions in combination with ethanol precipitation. For viral time course experiment, hearts were homogenized on a Bead Mill 4 (Thermo Fisher) and digested using DNeasy blood and tissue kit (Qiagen) according to manufacturer's instructions.

For detection of viral genomes, qPCR was performed with SYBR Select Master Mix for CFX (Thermo Fisher) on a QuantStudio 6 Flex System (Thermo Fisher). Cellular genome DNA reference gene C1 primer forward- 5'-CCT TCC AGT TGA GTC AGT GG-3' reverse- 5'-CTG CTG CTG TTG GGT ACT TC-3'. For detection of MAdV-3 viral genomes, MAdV3 qPCR-2.FORWARD: GTG GGA GGA TTT GAG GAG ATG; MAdV3 qPCR-2.REVERSE: ATG TAG CAC AGG CAT TAG TAG G were employed.

RNA extraction and RT-qPCR

Tissue was homogenized in TRIzol (Thermo Fisher) and clarified by phenol-chloroform phase separation according to manufacturer's instructions. RNA was further purified with the PureLink RNA Mini Kit (Thermo Fisher) and DNA was removed by on column DNase digestion. cDNA was generated with iScript Reverse Transcription Supermix for RT-qPCR (Bio-Rad) according to manufacturer's instructions. Real-time PCR was performed with SYBR Select Master Mix for CFX (Thermo Fisher) on a QuantStudio 6 Flex System employing the following primers: *Hprt*

Mm.PT.39a.22214828 IDT; *Cacna1c*, Mm.PT.58.8608981 IDT; *Scn5a*, Mm.PT.58.30418114 IDT; *Kcnh2*, Mm.PT.58.42865919 IDT; *Cdh2*, Mm.PT.58.12378183 IDT; *Pkp2*, Mm.PT.58.11914062 IDT; T*jp1*, Mm.PT.58.12952721 IDT; *Gja1*, Mm.PT.58.5955325 IDT; *Gjc1*, Mm.PT.58.8383900 IDT.

Langendorff heart preparations and optical mapping

Animals were anesthetized and cervical dislocation performed upon loss of peripheral stimuli response and immediately followed by thoracotomy and cardiac excision. Hearts were cannulated and Langendorff-perfused within 4 min, as previously described[74]. Hearts were perfused with a pH = 7.4 baseline crystalloid solution containing (in mM): NaCl (144.5), $CaCl_2$ (1.8), NaOH (5.5), KCl (4), Dextrose (5.5), $MgCl_2$ (1), HEPES (10), NaH_2PO_4 (1.2). Solutions were bubbled with 100% O2 for the duration of the experiment and run at a constant flow to maintain a pressure of ~70-90 mmHg, with perfusates and the tissue bath maintained at 37 °C. Following a 15 min stabilization period, hearts were perfused with 8 μM Di-4-ANEPPS (Biotium), excess dye was washed out over a 20 min period, and images acquired during subsequent perfusion. The electromechanical uncoupler blebbistatin (10 μM, ApexBio Tech), as well as slight pressure on the posterior surface of the heart, were used to minimize cardiac motion and stabilize the heart against the glass of the imaging window. Hearts were paced with a unipolar silver wire placed on the anterior epicardium and a reference wire placed in the back of the bath. Stimulation at 1.5 X the diastolic threshold was applied at a basic cycle length of 150 ms and 1-2 ms pulse duration. Hearts were paced for 30 sec before each image was collected. Action potentials were recorded as previously described[75]. Briefly, the anterior epicardium of the heart was illuminated by a light-emitting diode (LED) light source (LEX3G, SciMedia) with a 520/35 nm band-pass filter (Brightline), and reflected onto the heart via epi-illumination using a 565 nm dichroic mirror (Chroma Technology). Emitted light was collected via a tandem lens system and transmitted through a 610 nm long-pass filter (Andover Corp.) before detection with a MiCAM Ultima L-type CMOS or 02CMOS camera (SciMedia). Action potentials were recorded at a sample rate of 1 kHz for a duration of 2 sec during intrinsic activity and steady state pacing. Conduction velocity (CV) was collected in the transverse and longitudinal direction (CVT and CVL, respectively), and was calculated as previously described[74]. Briefly, activation time for each pixel was designated as the maximum rate of rise of the optical action potential. Conduction in each direction was quantified by selecting vectors up to 5 pixels away and within an angle of ± 8° from a user-defined line indicating the direction of action potential propagation. Conduction vectors within 2 rows of the pacing site were excluded to reduce pacing artifacts. Data are presented as representative isochrone maps with 2 ms time steps and summary data (mean ± SEM).

Western blotting

Mouse hearts were homogenized in RIPA buffer (50 mM Tris pH 7.4, 150 mM NaCl, 1 mM EDTA, 1 % Triton X-100, 1 % sodium deoxycholate, 2 mM NaF, 200 μM Na_3VO_4, 0.1 % sodium dodecyl sulfate, 5 mM *N*-ethylmaleimide; all from Sigma Aldrich) supplemented with HALT protease and phosphatase inhibitor cocktail (Thermo Fisher). Lysates were clarified by sonication and centrifugation and concentration determined by DC protein assay (Bio-Rad). 4X Bolt LDS sample buffer (Thermo Fisher) supplemented with 400 mM DTT (Sigma Aldrich) was added to samples then heated to 70 °C for 10 min and subjected to SDS-PAGE using NuPAGE Bis-Tris 4-12 % gradient gels with MES (Thermo Fisher) running buffer according to manufacturer's instructions. Proteins were transferred to LF-PVDF (Bio-Rad) membrane and fixed in methanol and dried. PVDF membranes were reactivated in methanol followed by blocking in 5 % nonfat milk (Carnation) or 5 % bovine serum albumin (Fisher Scientific) in TNT buffer (0.1 % Tween 20, 150 mM NaCl, 50 mM Tris pH 8.0) for 1 h at room temperature. Primary antibodies were incubated overnight at 4 °C utilizing: rabbit anti-Cx43 (1:3,000; Sigma-

Aldrich), mouse anti-GAPDH (1:2,000; Santa Cruz Biotechnology), mouse anti-α-tubulin (1:3,000; Sigma Aldrich), rabbit mAb [D3H8Q] anti-V5 (1:1,000; Cell Signaling Technology), rabbit anti-HAdV-5 (1:5,000; Abcam), and rabbit mAb [D6W8P] anti-phospho-Cx43^{Ser368} (1:1,000; Cell Signaling Technology). Membranes were washed six times with 1 X TNT before secondary antibody labeling. Membranes were labeled for 1 h at room temperature with secondary antibodies conjugated with AlexaFluor555 or AlexaFluor647 (1:5,000; Thermo Fisher) or HRP (1:5,000; Abcam). For HRP labeling (phospho-Cx43^{Ser368}), membranes were stripped for 30 min in ReBlot Plus Strong Antibody Stripping Solution (Sigma Aldrich) before reprobing for total Cx43. Membranes were imaged and quantified utilizing a Chemidoc MP imaging system with Image Lab software (Bio-Rad).

Patch clamping

Electrophysiological recordings from dissociated cardiomyocytes were performed at room temperature using whole-cell voltage-clamp and current-clamp techniques. Recordings were made with an Axopatch 200B amplifier, Digidata 1550B digitizer, and pClamp 11 software (Molecular Devices) with a 20 kHz sampling rate and low-pass filtering at 5 kHz. Series resistance was monitored and compensated at > 70 % during voltage-clamp recordings. Recording electrodes with a tip resistance of 2-4 MΩ were pulled from borosilicate glass. Action potentials and potassium currents (I_{K1}, I_{Ks}, and I_{Kr}) were recorded with an internal pipette solution containing (mM): K-aspartic acid (120), KCl (20), NaCl (10), $MgCl_2$ (2), and HEPES (5) brought to pH 7.3 with KOH, and extracellular solution containing (mM): NaCl (120.4), KCl (12.7), KH_2PO_4 (0.6), Na_2HPO_4 (0.6), $MgSO_4$-$7H_2O$ (1.2), $NaHCO_3$ (4.6), Taurine (30), Glucose (5.5), and HEPES (10) brought to pH 7.4 with HCl. Sodium current and calcium currents were recorded with an internal pipette solution containing (mM): $CsMeSO_3$(120), tetraethylammonium chloride (20), $MgCl_2$ (2), HEPES (10), EGTA (10), and Mg-ATP (4) brought to pH 7.3 with CsOH. Sodium currents were recorded in extracellular solution containing (mM): NaCl (25), N-methyl-D-glucamine (120), $CaCl_2$ (1.8), $MgCl_2$ (1.8), glucose (10), and HEPES (10), pH 7.3, supplemented with 1 μM nisoldipine to block voltage-gated calcium channels. Calcium currents were recorded in extracellular solution containing (mM): NaCl (137), CsCl (5.4), $MgCl_2$ (1.8), $CaCl_2$ (2), glucose (10), and HEPES (10), pH 7.3, supplemented with 10 μM TTX to block voltage-gated sodium channels.

Resting membrane potential and action potentials were recorded in current-clamp mode. RMP was measured by averaging the membrane potential across 5 seconds with no current injection. Action potentials were recorded with the membrane potential held at -90 mV by a constant bias current and elicited by 2 ms current pulses between 200 pA to 2 nA at 1 sec intervals. Action potential shape analysis was performed on action potentials elicited in response to the lowest current injection using the Action Potential module in Clampfit 11 (Molecular Devices). I_K, I_{Na}, and I_{Ca} were recorded in voltage-clamp mode, and the 10 mV liquid junction potential was corrected for during the recordings. I_{K1} was elicited from a holding potential of -40 mV with 2.5 sec depolarizing voltage steps from -100 mV to 0 mV and quantified by measuring the peak steady-state current amplitude during the voltage steps. To measure I_{Ks} and I_{Kr}, cardiomyocytes were held at a holding potential of -40 mV holding potential, given depolarizing voltage pulses from -30 to 60 mV for 2.5 sec, and then stepped back to -40 mV in the absence and presence of 5 μM E4031 (Cayman chemical). I_{Ks} was determined by measuring the peak amplitude of the tail current in the presence of E4031, and I_{Kr} was determined by measuring the peak amplitude of the E4031-sensitive current. I_{Na} was elicited from a holding potential of -90 mV with 20 ms depolarizing steps from -80 mV to +60 mV. I_{Ca} was recorded from a holding potential of -40 mV with 300 ms depolarizing steps from -30 mV to +60 mV. I_{Na} and I_{Ca} were determined by measuring the peak current amplitude relative to baseline during the voltage steps. Three runs were completed per cell for all recordings.

Immunofluorescence microscopy
As previously described[38,76,77], cells were fixed with -20 °C methanol for 5 min, washed, and blocked with 5 % normal goat or donkey serum (Thermo Fisher) containing 0.1 % Triton X-100 (Sigma Aldrich) which was increased to 0.5 % for ACMs for 1 h at room temperature. Primary antibody labeling was performed for 1 h at room temperature using; rabbit anti-Cx43 (1:3,000; Sigma), goat anti-Cx43 (1:250; Abcam), rabbit mAb [D6W8P] anti-phospho-Cx43^{Ser368} (1:1,000; Cell Signaling Technology), mouse anti-N-Cadherin (1:250; BD Biosciences), mouse anti-Adenovirus E1A [M73] (1:2,000; Abcam), rat anti-F4/80 (1:250; Abcam), rabbit anti-CD3 (1:250; Novus), or goat anti-CD45R (1:500; Novus). Cells was washed 6 times prior to labeling for 1 h at room temperature with fluorescently-conjugated secondary antibodies raised in goat (AlexaFluor 488, 555, or 647; 1:500; Thermo Fisher) or donkey (AlexaFluor 488 or 647; 1:500; Jackson Labs and CF568; 1:500; Biotium) and counterstained with DAPI (Thermo Fisher). Immunofluorescence of tissue was performed on 8 µm acetone-fixed cryosections from snap frozen tissue in OCT as previously described[77]. The labeling protocol was the same as for cells with the modification of overnight incubation with primary antibodies at 4 °C overnight and inclusion of 0.05% Tween 20 (Fisher Scientific) in 2 initial washes following primary and secondary antibody incubations. Confocal imaging was performed on SoRa Spinning Disk (Nikon) or Opterra swept field confocal microscope (Bruker) and image processing was undertaken using FIJI software (NIH)[78]. SoRa images were deconvolved and processed utilizing NIS-Elements Advanced Research software (Nikon) and Bruker Opterra confocal image processing was undertaken using FIJI software (NIH)[78]. Colocalization of N-cadherin and Cx43 was assessed via Pearson's and Mander's correlation coefficient across the Z-stack. Antibody specificity was confirmed through inclusion of secondary-only controls. Additionally, optimization and experimental cardiac CD3, CD45R, and F4/80 immunostaining was performed in tandem with spleen tissue sections to confirm both specificity and successful labeling. Acquisitions and analyses were performed blind with fields of view chosen at random within areas of interest (e.g. left ventricle) and representative images presented were chosen to reflect that concluded by averaged summary data.

Live calcium transients imaging
HiPSC-CMs were plated into 35 mm glass bottom culture dishes (Cellvis) and maintained as described above to form monolayers and mature. Cells were infected with HAdV-5 at an MOI of 10 and loaded with Fluo-4AM (Thermo Fisher) diluted in Tyrode's solution containing (mmol/L): NaCl (140), KCl (5.4), $MgCl_2$ (1), sodium pyruvate (2), $CaCl_2$ (1), glucose (10), HEPES (10), pH adjusted to 7.4 using NaOH at room temperature[79]. Live cell imaging was performed utilizing an Opterra swept field confocal microscope (Bruker) with a 20x objective with an acquisition rate of 166.67 Hz for at least 6 fields of view per well encompassing several spontaneous firings. Fluorescence from image sequences encompassing one field of view was normalized in FIJI[78] by generating maximum (MaxIP) and minimum (MinIP) intensity projections, and subtracting MinIP from the original image sequence and MaxIP. The resulting image sequence was divided by the result of MaxIP-MinIP. Regions of interest (ROIs) were defined over individual cells and fluorescence intensity plotted over time. ROIs were selected at random from cells that were firing during a 2.916 second-long live cell imaging series. ROI were kept size-consistent across all image analysis and acquired data from the cytosolic space of cells. Standard deviation of timepoint for peak fluorescence intensity of one firing from 4 cells in each sequence was calculated as a measure of synchronicity.

Statistics
All experiments were repeated at least three times and blinding of data was implemented prior to quantification (see figure legends for specific replicate values). All technical replicates are

averaged into single data points, so only biological replicates are presented. Data are presented as mean ± SEM. Statistical analysis was conducted with GraphPad Prism (GraphPad Software, Inc.). A value of $p<0.05$ was considered statistically significant.

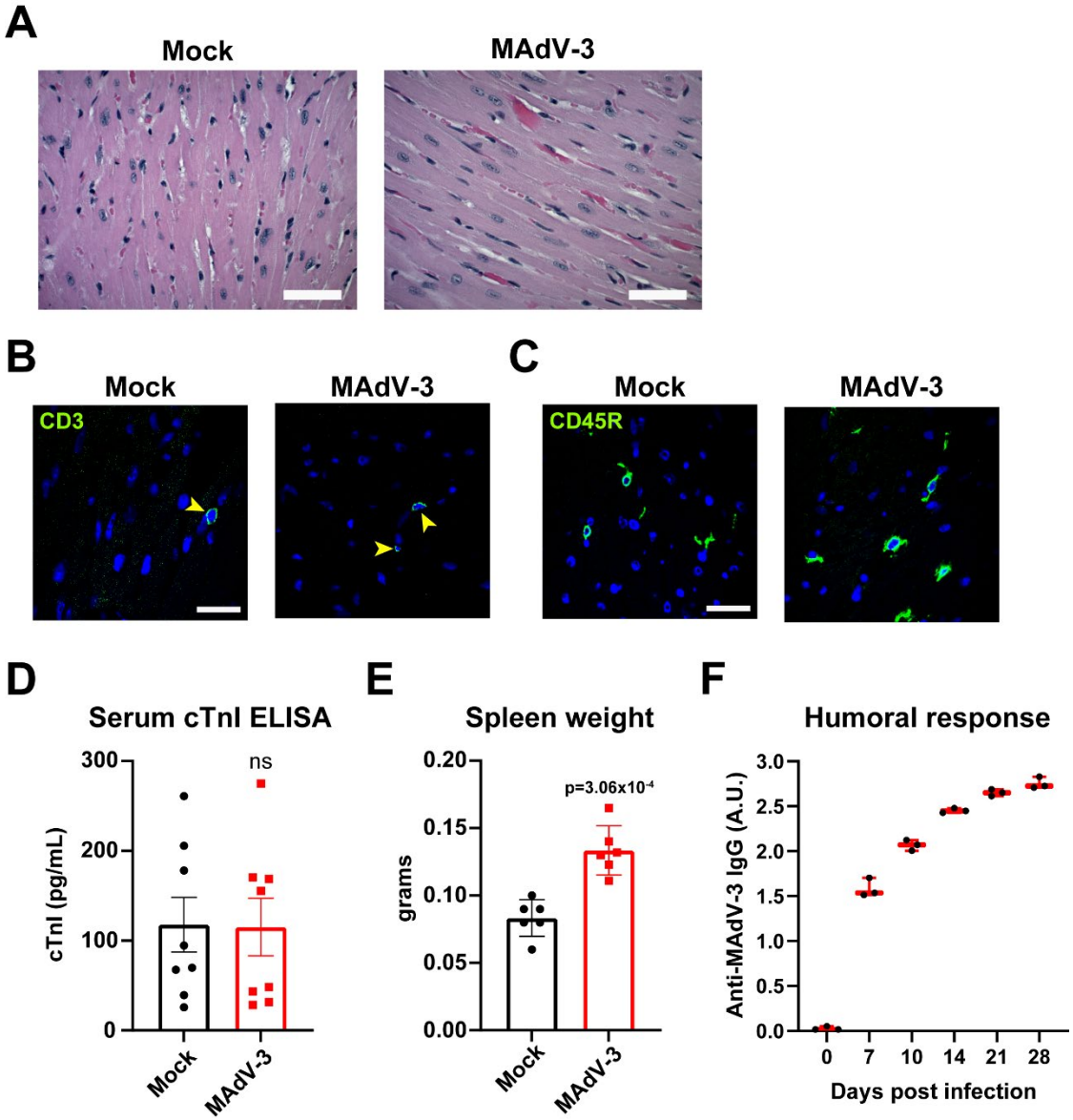

Supplemental Figure 1. Acute MAdV-3 infection does not induce inflammatory cardiomyopathy but does increase spleen weight and elicit a humoral response. Mice were infected retro-orbitally with $5x10^5$ i.u. MAdV-3 or saline (mock) and spleen tissue or serum was harvested 7 d.p.i. for analyses. **A)** Histopathology by H&E staining on paraffin embedded cardiac sections (scale bar: 50 µm). **B)** Confocal immunofluorescence microscopy of ventricular cryosections labeled for infiltrating T-lymphocytes (CD3, green; scale bar: 25 µm). **C)** Confocal immunofluorescence microscopy of ventricular cryosections labeled for infiltrating B-lymphocytes (CD45R, green; scale bar: 25 µm). **D)** Cardiac troponin I ELISA from circulating blood serum of mock or MAdV-3 infected mice was quantified (n=8). **E)** Gross spleen weights (n=6). **F)** Anti-MAdV-3 mouse IgG ELISA from serum to detect humoral immune responses (n=3). ***$p = 3.06x10^{-4}$, student's t-test. Data are represented as mean ± SEM.

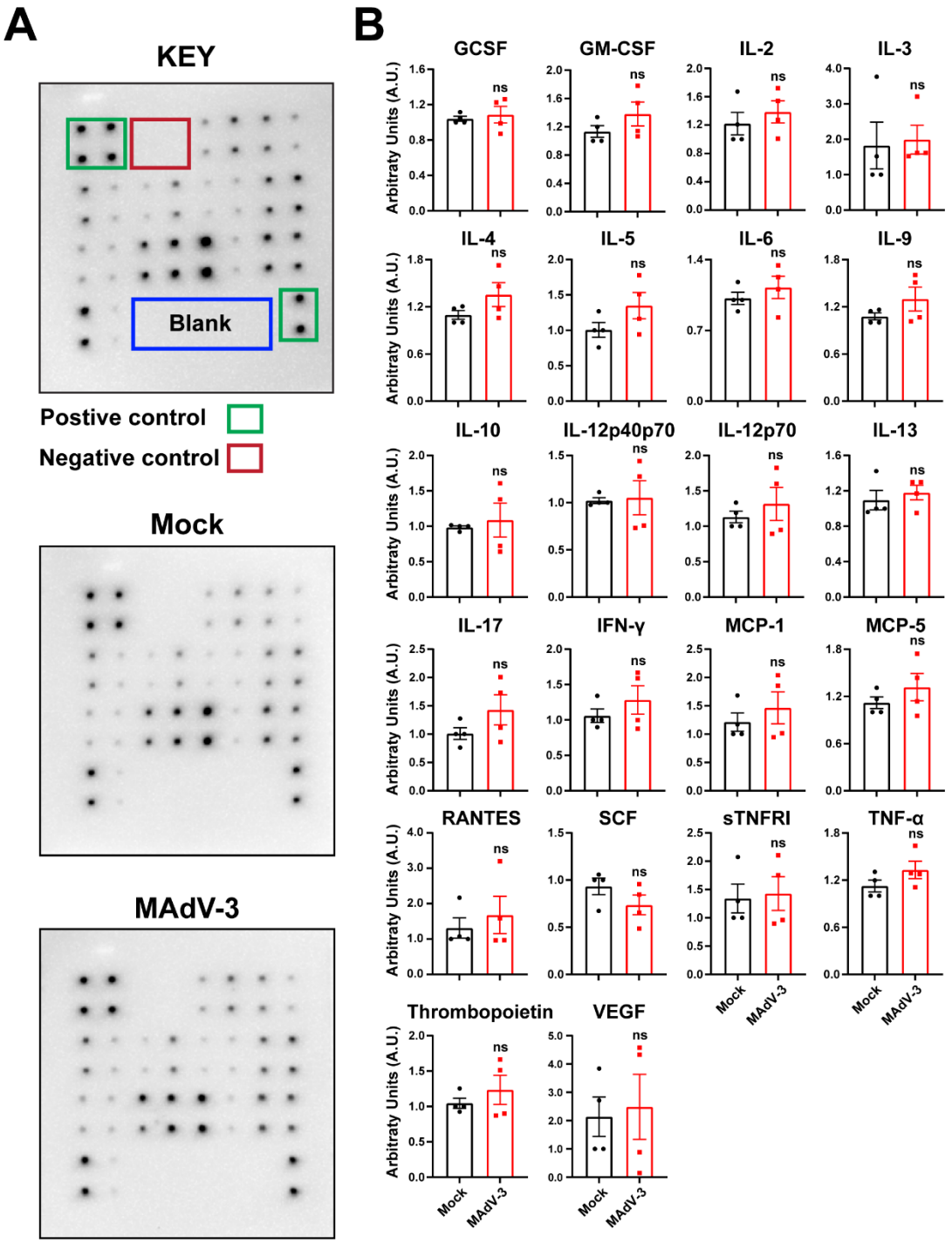

Supplemental Figure 2. Acute MAdV-3 infection does not elicit a detectable cytokine response in the heart 7 days post infection. Mice were infected retro-orbitally with $5x10^5$ i.u. MAdV-3 or saline (mock) and cardiac tissue was harvested 7 d.p.i. for analyses. **A)** Representative whole blot images from cytokine array performed on cardiac tissue lysate. **B)** Quantification of blots from cytokine array (n=4). Student's t-test. Data are represented as mean ± SEM.

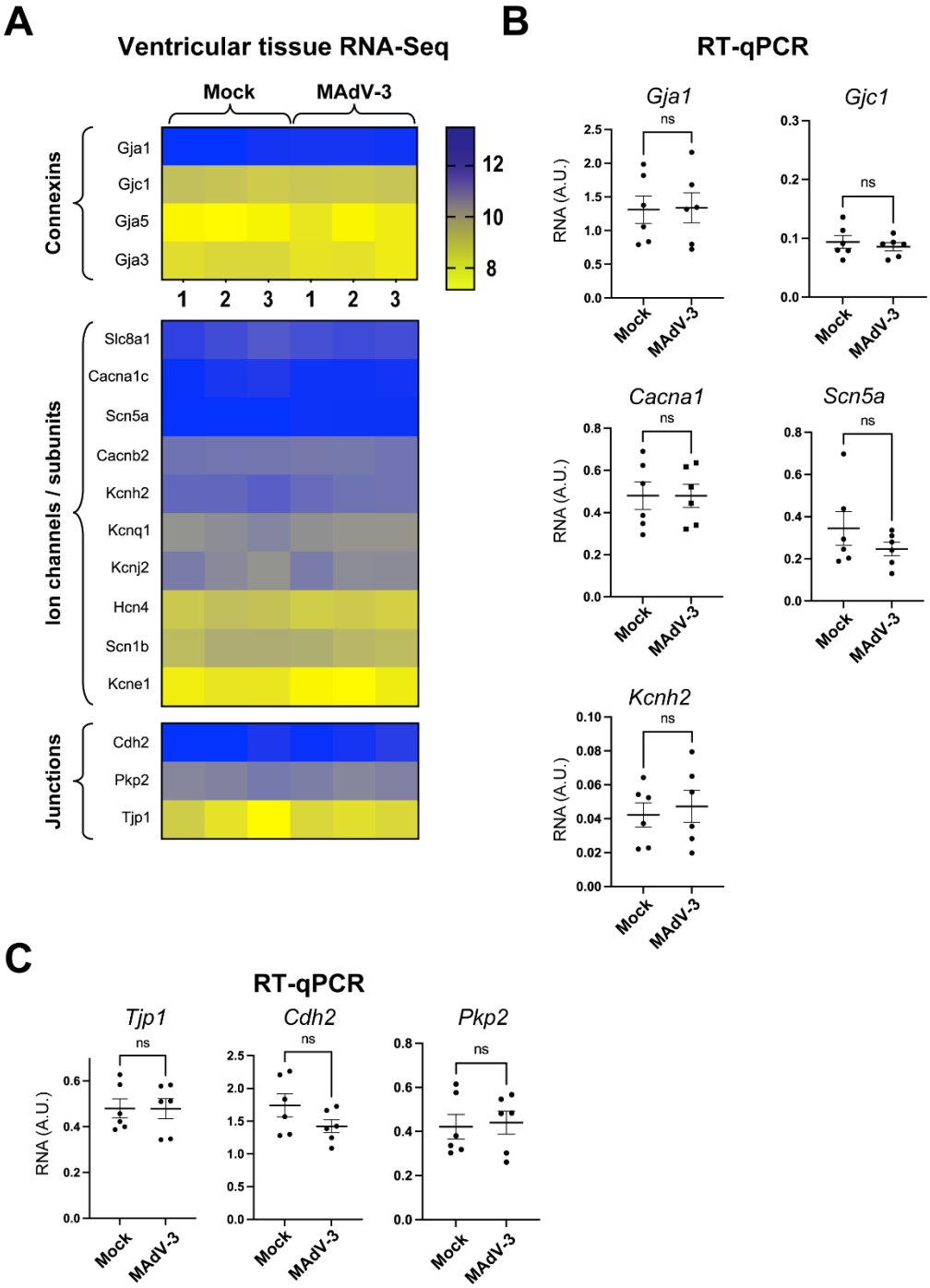

Supplemental Figure 3. Acute adenovirus infection does not alter gene expression of major cardiac electrophysiological and structural proteins. Mice were infected retro-orbitally with $5x10^5$ i.u. MAdV-3 or saline (mock) and cardiac tissue was harvested 7 d.p.i. for analyses. **A)** Heat map of RNA-Seq data for major cardiac connexins, ion channels and subunits, and intercalated disc encoding mRNAs (n=3). **B)** RT-qPCR of heart tissue mRNA for *Gja1*, *Gjc1*, *Cacna1*, *Scn5a*, and *Kcnh2* (n=6). **C)** RT-qPCR of heart tissue mRNA for major cardiac scaffolding genes *Cdh2*, *Pkp2*, and *Tjp1*, (n=6). student's t-test. Data are represented as mean ± SEM.

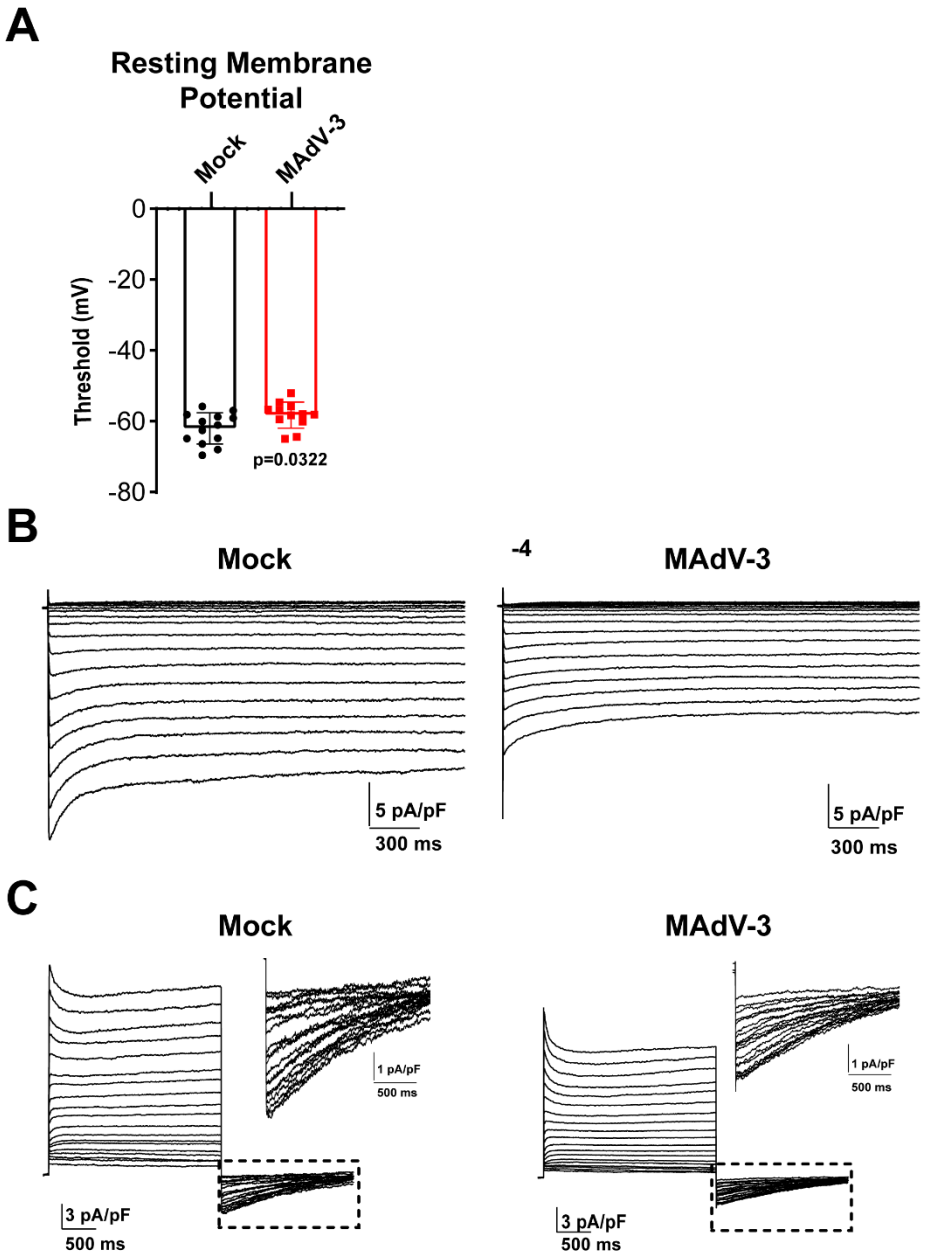

Supplemental Figure 4. Cellular resting membrane potentials and raw traces of I_{K1} and I_{Ks} currents. Isolated ACMs were infected with MAdV-3 at MOI 10 and were patch clamped at 24 h.p.i., **A)** Resting membrane potentials recorded from mock or infected isolated ACMs (student's t-test p = 3.22×10^{-2} n=13,12). **B)** Full current traces of I_{K1} in uninfected and infected cardiomyocytes. **C)** I_{Ks} insert currents measured in the presence of 5 μM E4031, n=19.

Supplemental Movies 1 and 2. Related to Figure 7. HiPSC-CMs were infected with HAdV-LacZ or HAdV-5 at an MOI 10 and harvested 24 h.p.i. Live-cell confocal microscopy 24 h.p.i. using Fluo-4 AM to measure Ca^{2+} transients was performed at 166 Hz.

References

62. Huang GY, Xie LJ, Linask KL, Zhang C, Zhao XQ, Yang Y, Zhou GM, Wu YJ, Marquez-Rosado L, McElhinney DB, et al. Evaluating the role of connexin43 in congenital heart disease: Screening for mutations in patients with outflow tract anomalies and the analysis of knock-in mouse models. J Cardiovasc Dis Res. 2011;2:206-212. doi: 10.4103/0975-3583.89804
63. Smyth JW, Vogan JM, Buch PJ, Zhang SS, Fong TS, Hong TT, Shaw RM. Actin cytoskeleton rest stops regulate anterograde traffic of connexin 43 vesicles to the plasma membrane. Circulation research. 2012;110:978-989. doi: 10.1161/CIRCRESAHA.111.257964
64. Burridge PW, Holmstrom A, Wu JC. Chemically Defined Culture and Cardiomyocyte Differentiation of Human Pluripotent Stem Cells. Curr Protoc Hum Genet. 2015;87:21 23 21-21 23 15. doi: 10.1002/0471142905.hg2103s87
65. Burridge PW, Matsa E, Shukla P, Lin ZC, Churko JM, Ebert AD, Lan F, Diecke S, Huber B, Mordwinkin NM, et al. Chemically defined generation of human cardiomyocytes. Nat Methods. 2014;11:855-860. doi: 10.1038/nmeth.2999
66. Buikema JW, Lee S, Goodyer WR, Maas RG, Chirikian O, Li G, Miao Y, Paige SL, Lee D, Wu H, et al. Wnt Activation and Reduced Cell-Cell Contact Synergistically Induce Massive Expansion of Functional Human iPSC-Derived Cardiomyocytes. Cell Stem Cell. 2020;27:50-63 e55. doi: 10.1016/j.stem.2020.06.001
67. Feyen DAM, McKeithan WL, Bruyneel AAN, Spiering S, Hormann L, Ulmer B, Zhang H, Briganti F, Schweizer M, Hegyi B, et al. Metabolic Maturation Media Improve Physiological Function of Human iPSC-Derived Cardiomyocytes. Cell reports. 2020;32:107925. doi: 10.1016/j.celrep.2020.107925
68. Green M, Loewenstein PM. Human adenoviruses: propagation, purification, quantification, and storage. Curr Protoc Microbiol. 2006;Chapter 14:Unit 14C 11. doi: 10.1002/9780471729259.mc14c01s00
69. O'Connell TD, Rodrigo MC, Simpson PC. Isolation and culture of adult mouse cardiac myocytes. Methods in molecular biology. 2007;357:271-296. doi: 10.1385/1-59745-214-9:271
70. Fernandez NF, Gundersen GW, Rahman A, Grimes ML, Rikova K, Hornbeck P, Ma'ayan A. Clustergrammer, a web-based heatmap visualization and analysis tool for high-dimensional biological data. Sci Data. 2017;4:170151. doi: 10.1038/sdata.2017.151
71. Wu T, Hu E, Xu S, Chen M, Guo P, Dai Z, Feng T, Zhou L, Tang W, Zhan L, et al. clusterProfiler 4.0: A universal enrichment tool for interpreting omics data. Innovation (Camb). 2021;2:100141. doi: 10.1016/j.xinn.2021.100141
72. Smyth JW, Fleeton MN, Sheahan BJ, Atkins GJ. Treatment of rapidly growing K-BALB and CT26 mouse tumours using Semliki Forest virus and its derived vector. Gene Ther. 2005;12:147-159. doi: 10.1038/sj.gt.3302390
73. Lindsey ML, Escobar GP, Mukherjee R, Goshorn DK, Sheats NJ, Bruce JA, Mains IM, Hendrick JK, Hewett KW, Gourdie RG, et al. Matrix metalloproteinase-7 affects connexin-43 levels, electrical conduction, and survival after myocardial infarction. Circulation. 2006;113:2919-2928. doi: 10.1161/CIRCULATIONAHA.106.612960
74. George SA, Sciuto KJ, Lin J, Salama ME, Keener JP, Gourdie RG, Poelzing S. Extracellular sodium and potassium levels modulate cardiac conduction in mice heterozygous null for the Connexin43 gene. Pflugers Arch. 2015;467:2287-2297. doi: 10.1007/s00424-015-1698-0
75. King DR, Entz M, 2nd, Blair GA, Crandell I, Hanlon AL, Lin J, Hoeker GS, Poelzing S. The conduction velocity-potassium relationship in the heart is modulated by sodium and calcium. Pflugers Arch. 2021;473:557-571. doi: 10.1007/s00424-021-02537-y

76. Smyth JW, Shaw RM. Autoregulation of connexin43 gap junction formation by internally translated isoforms. Cell reports. 2013;5:611-618. doi: 10.1016/j.celrep.2013.10.009
77. Zeitz MJ, Calhoun PJ, James CC, Taetzsch T, George KK, Robel S, Valdez G, Smyth JW. Dynamic UTR Usage Regulates Alternative Translation to Modulate Gap Junction Formation during Stress and Aging. Cell reports. 2019;27:2737-2747 e2735. doi: 10.1016/j.celrep.2019.04.114
78. Schindelin J, Arganda-Carreras I, Frise E, Kaynig V, Longair M, Pietzsch T, Preibisch S, Rueden C, Saalfeld S, Schmid B, et al. Fiji: an open-source platform for biological-image analysis. Nat Methods. 2012;9:676-682. doi: 10.1038/nmeth.2019
79. Walter A, Saric T, Hescheler J, Papadopoulos S. Calcium Imaging in Pluripotent Stem Cell-Derived Cardiac Myocytes. Methods in molecular biology. 2016;1353:131-146. doi: 10.1007/7651_2015_267